POLITECNICO DI TORINO

MASTER THESIS IN ELECTRICAL ENGINEERING

A.Y. 2024/2025

Design and simulation of REE free Variable Flux Machine





Author:

Vittorio Fabbricatore

Supervisors:

Gianmario Pellegrino

Michela Diana

Paolo Pescetto

Simone Ferrari

Index

In	trodu	ction and Motivation	1
1	Bacl	kground and Case Study	2
	1.1	PMSM	2
	1.2	Variable Flux Machine (VFM)	4
	1.3	Software in use	8
	1.4	Design Requirements and Specifications	10
	1.5	Reference Case Study	11
2	Proj	posed Design Methodology	13
	2.1	Motor Model	13
	2.2	JMAG Setup	14
	2.3	Optimization First Method	17
		2.3.1 Study	17
		2.3.2 Optimization Setting	18
		2.3.3 Pareto Set Analysis	20
		2.3.4 Results	21
	2.4	Optimization Second Method	23
		2.4.1 Study	23
		2.4.2 Optimization Setting	24
		2.4.3 Pareto Set Analysis	26
		2.4.4 Results	27
		2.4.5 Selection of the Final Solution	29
	2.5	Reuse Demagnetization condition	30
	2.6	Conclusion	33
3	Mot	or Analysis	34
	3.1	Demagnetization/Remagnetization Maps	36
	3.2	Flux maps and Torque curve	38
	3.3	Remagnetization voltage limit	42
	3.4	Efficiency maps	46

3.5	Drive Cycle	50
3.6	Cost Analysis and Environmental Load Unit (ELU)	53
3.7	Conclusion and Future Works	55

Introduction and Motivation

The transition to sustainable mobility is accelerating the demand for high-performance electric machines. While Permanent Magnet Synchronous Machines (PMSMs) are widely adopted for their efficiency and controllability, their reliance on rare earth elements (REEs) raises environmental and supply chain concerns. To overcome these limitations, research is focusing on REE-free solutions and innovative topologies such as Variable Flux Machines (VFMs), which use low-coercivity magnets that can be actively demagnetized and remagnetized during operation.

This thesis, carried out in collaboration with Volvo Cars Corporation (Sweden), investigates the design of a REE-free VFM for automotive applications. The study employs a new rare-earth-free iron nitride permanent magnets and establishes a systematic workflow combining JMAG for finite element optimization and SyR-e for parametric analysis.

The primary aim of this work is to define a design methodology for the realization of an electrical machine suitable for automotive application, combining high performance with reduced environmental impact. By exploiting REE-free permanent magnets and advanced optimization tools, the proposed approach seeks to deliver a motor design that is both technically competitive and aligned with the ongoing transition to sustainable mobility.

1 Background and Case Study

1.1 PMSM

Permanent Magnet Synchronous Machines (PMSMs) are among the most widely adopted and efficient solutions for electric traction and advanced industrial applications. Their defining feature is the use of permanent magnets on the rotor, which generate the magnetic field required for operation without the need for rotor currents. This design reduces losses, increases torque density, and improves overall performance.

From a topological perspective, PMSMs can be classified into three main configurations:

- Surface-mounted PMSM (SPM): magnets are mounted directly on the surface of the rotor, resulting in an isotropic magnetic design where torque is mainly generated by the magnets.
- Interior Permanent Magnet (IPM) motors: magnets are embedded within the rotor, allowing a combination of magnet torque and reluctance torque.
- Permanent Magnet-assisted Synchronous Reluctance (PM-SyR) motors: most of the torque is generated by reluctance, with the magnets providing only a minor contribution.

The selected topology significantly affects efficiency, power density, and the control strategy required for optimal operation.

From a modeling standpoint, electrical and magnetic quantities are initially expressed in the three-phase abc reference frame, which represents currents, voltages, and flux linkages. For simplified analysis and control, linear transformations are applied to switch to equivalent frames such as the $\alpha\beta$ and, most importantly, the dq frame, where the d-axis aligns with the magnet flux and the q-axis is orthogonal to it. In this reference frame, the electromagnetic torque can be expressed as the sum of two components: one provided by the magnets and another by reluctance. While SPM machines primarily rely on the magnet torque, IPM and PM-SyR machines exhibit a significant reluctance torque contribution as well.

To fully exploit the machine's performance, advanced control strategies are often implemented. The Maximum Torque Per Ampere (MTPA) strategy maximizes the torque delivered for a given current, while the Maximum Torque Per Volt (MTPV) strategy becomes essential at high speeds, where the inverter voltage limit becomes the main constraint.

The selection of permanent magnets is a critical aspect in PMSM design, as it determines not only torque density and specific power but also the operational limits related to demagnetization. Key magnetic properties include:

- Remanence, which quantifies the residual flux retained by the magnet;
- Coercivity, which measures the magnet's resistance to external demagnetizing fields;
- The maximum energy product BH_{max} , which provides an indication of the magnetic energy stored per unit volume.

It is crucial that the operating point of the magnet remains above the knee point of the BH curve to prevent irreversible demagnetization, which would otherwise compromise the performance and reliability of the machine.

1.2 Variable Flux Machine (VFM)

A Variable Flux Machine (VFM) is a permanent magnet machine characterized by its ability to actively regulate the magnetic flux during operation. This regulation is achieved through the reversible demagnetization and remagnetization of low-coercivity magnets, using current injection along the d-axis: negative current for demagnetization and positive current for remagnetization.

The adoption of VFMs is motivated by two main advantages. From an environmental perspective, these machines enable a reduction in the use of rare-earth elements (REE), contributing to a more sustainable design. From an electrical performance standpoint, VFMs extend the machine's speed range, thereby improving efficiency across different operating conditions [1].

As illustrated in Fig.1.1, when the magnet is partially demagnetized, the maximum torque decreases (orange curve), but the achievable speed increases. This allows typical operating points in automotive applications to be shifted into a region of higher efficiency (orange area).

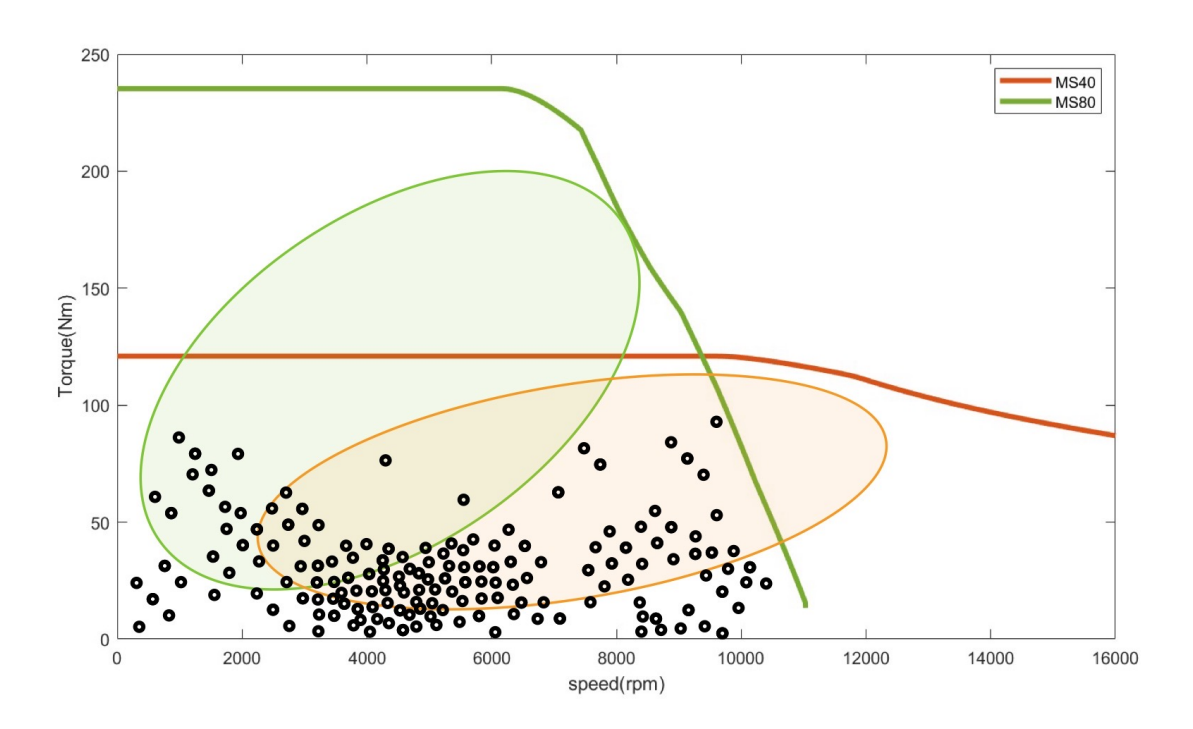


Figure 1.1: Typical automotive working points

The key enabler of VFMs is the use of low-coercivity magnets. Their main advantage lies in the ease of regulation, as they require significantly lower currents compared to high-coercivity magnets to undergo demagnetization and remagnetization. However, they also present

drawbacks, such as a reduced maximum torque and increased susceptibility to demagnetization under active short-circuit (ASC) conditions, where there is a risk of complete magnetization loss.

A comparison of different REE-free magnets is summarized in Fig.1.2. For instance, AlNiCo magnets require low currents for flux variation and offer higher flux density compared to SmCo, but they are more expensive and particularly prone to demagnetization. On the other hand, SmCo magnets provide a more linear demagnetization characteristic, though with a lower flux density [2].

Magnet Type	Br (T)	αBr (%/K)	Hc (kA/m)	Hcj (kA/m)	αHcj (%/K)	BHmax (kJ/m³)	ρ (10 ⁶ Ω·m)	Tmax (°C)
Ferrite 27/25SH	0.400	-0.20	278	302	+0.30	30	104	250
AlNiCo Cast 80/12	1.11	-0.01 ~ - 0.035	130	126	-0.03 ~ - 0.03	80	0.45 ~ 0.55	500
SmCo YXS24	1.02	-0.035	764	2000	-0.25	191	0.75 ~ 0.85	250
NdFeB N42SH	1.33	-0.11 ~ - 0.12	1018	1595	-0.56 ~ - 0.70	334	1.4 ~ 1.6	150

Figure 1.2: Magnet comparison

In this work, iron nitride magnets have been selected.

With regard to magnetization control methods, two approaches can be adopted. The first involves the use of an auxiliary winding, which simplifies the control strategy but requires additional space inside the machine. The second leverages the stator winding, thereby reducing hardware complexity and cost, but imposing higher demands on the inverter: the current pulses required for demagnetization, and especially for remagnetization, can be several times higher than the nominal current of the machine, even if applied for very short durations [2].

To monitor the state of the magnets, the concept of Magnetization State (MS) is introduced. MS is defined as the ratio between the current magnetic flux and the original flux (before any demagnetization), with MS = 100% representing a fully magnetized magnet [3].

$$MS = \frac{\lambda_m}{\lambda_{m,max}} \tag{1}$$

Flux regulation can thus be described in terms of controlled variation of MS. For example (Fig.1.3), to reduce MS from 100% to 50%, a negative d-axis current must be injected, moving the operating point along the trajectory P0–D2–P2. In this condition, the magnet exhibits reduced induction, resulting in lower torque. Conversely, to increase MS to 75%, a positive current must be applied, which drives the operating point along the path P2–R2–R1–P1. It is important to note that the remagnetization trajectory is significantly longer than the demagnetization one, implying that I_{remag} is typically much higher than I_{demag} , with a ratio that depends on the machine design.

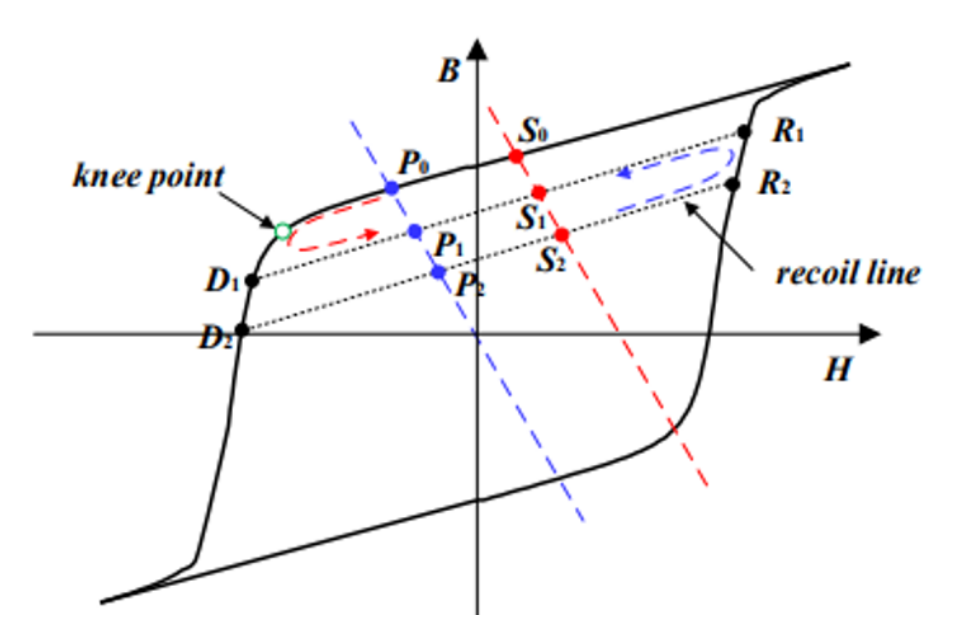


Figure 1.3: Flux regolation [4]

The Fig.1.4 compares different rotor configurations, highlighting the current requirements for flux variation. The orange bars represent the current needed to demagnetize the magnet down to 10% MS, while the yellow bars indicate the current required for remagnetization, both up to 100% (first column) and up to 90% (second column). Based on these results, the Surface-mounted Permanent Magnet (SPM) configuration was selected, as it provides the lowest I_{remag}/I_{demag} ratio. Moreover, the remagnetization target was set at 80% MS, as a compromise between torque recovery and current limitation [5].

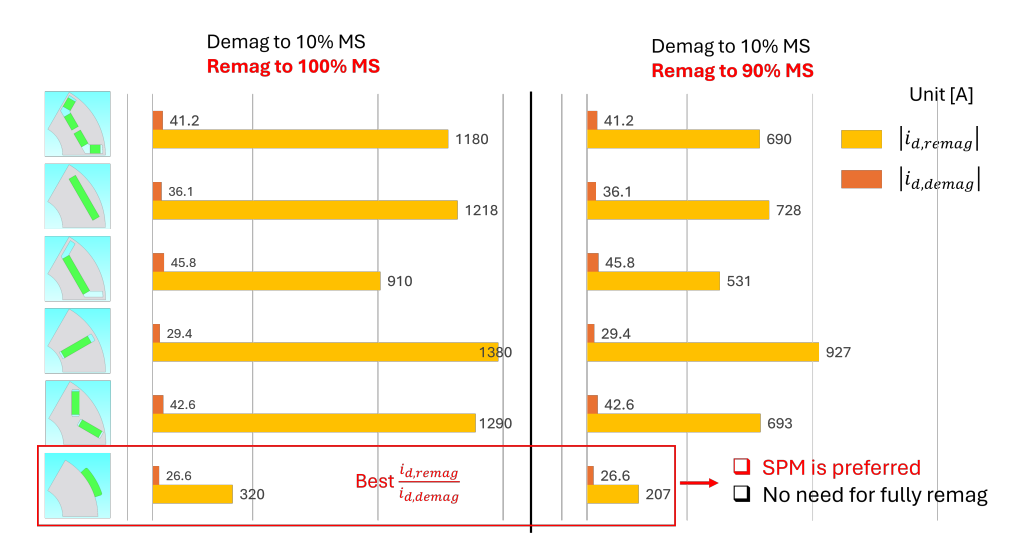


Figure 1.4: Rotor comparison [6]

1.3 Software in use

The design, simulation, and optimization activities carried out in this thesis relied on a combination of specialized software tools, each playing a distinct role within the workflow.

• SyR-e (Synchronous Reluctance – evolution) is an open-source software developed in the Matlab/Octave environment and distributed under the Apache 2.0 license. It enables the parametric design of synchronous machines, including variants with permanent magnets, by performing finite element analysis (FEA) through FEMM. On the design side, it integrates sizing equations, multi-objective optimization algorithms (such as differential evolution), and advanced post-processing tools. Primarily used in the early stages of parametric modeling and optimization, SyR-e allows an automated workflow from CAD model generation to simulation and performance evaluation [7].

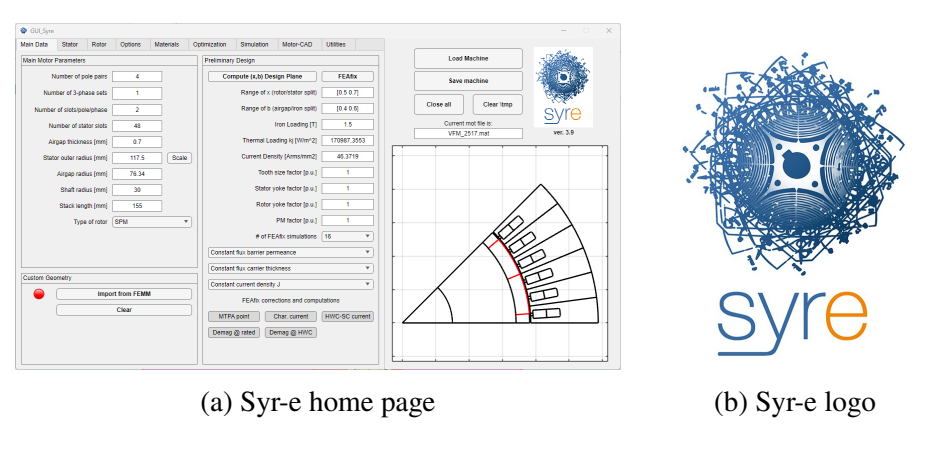
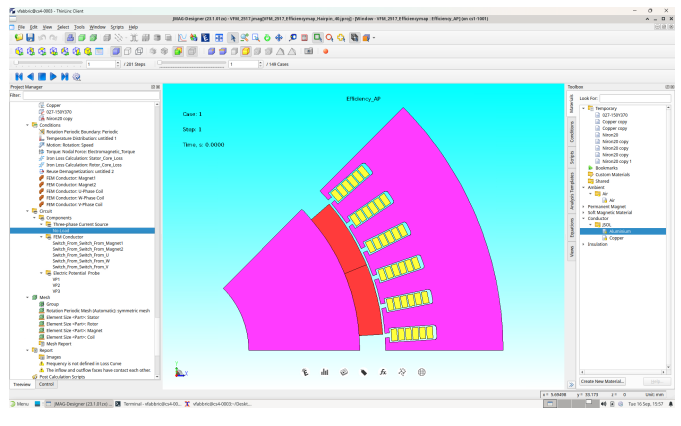


Figure 1.5

• JMAG is a commercial electromagnetic simulation software developed by JSOL Corporation, with the latest version known as JMAG-Designer 23.2. It offers powerful finite element (FEM) capabilities for electromagnetic, thermal, and structural phenomena, while also supporting integrated multiphysics simulations. Due to its advanced features and its interface with automation and drive circuitry tools, JMAG is extensively used in the automotive sector for the design of electric motors and drive systems. In this work, JMAG has served as the primary tool for advanced modeling, transient analysis, and optimization of the magnetic and mechanical behavior of the VFM.





(a) JMAG home page

(b) JMAG logo

Figure 1.6

 MATLAB is a numerical computing and programming environment widely used in both academia and industry for modeling, control, and data processing. Complemented by Simulink, a graphical platform for multi-domain simulation and model-based design, it enables the development of dynamic models, control simulations, embedded code generation, and Hardware-in-the-Loop (HIL) validation.

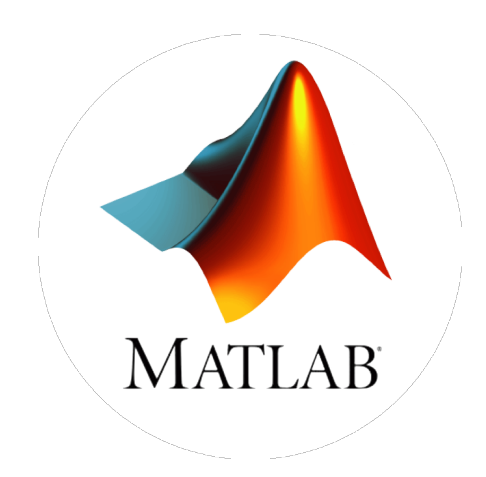


Figure 1.7: Matlab logo

1.4 Design Requirements and Specifications

The definition of design requirements and constraints represents the starting point of any electromechanical design activity. The requirements specify the performance targets that the machine must meet to be considered suitable for the intended application — for example, the minimum torque, the operating speed range, or the desired energy efficiency. The constraints, on the other hand, establish the limits within which the design must remain, such as geometric dimensions, thermal thresholds, or maximum allowable currents. Clearly defining these two sets of parameters is essential to effectively guide the subsequent phases of modeling and optimization, preventing unrealistic solutions or designs incompatible with real-world manufacturing. The following tables (Table1.1 and Table1.2) summarize the key requirements and constraints considered as reference for the development of this project.

Table 1.1: Requirements

Power	$>150 \; kW$
Torque	>250 Nm
Maximum Speed	$16000 \ rpm$
Supply Voltage	720~V

Table 1.2: Constraints

Gear Ratio	9-13
Stator Diameter	< 235
Stack Length	< 160
Airgap	$0.8{-}1.1 \ mm$
Hairpins	6

1.5 Reference Case Study

As a reference for this work, the IPM motor developed in the thesis of a former student (Satoshi Ghiba) was selected, as it was also designed using a combination of Neodimium and REE-free magnets [8]. The main design and performance characteristics of this machine are reported, supported by several representative graphs. In particular, the analysis includes the torque and power curves, the loss maps (total losses, iron losses, permanent magnet losses, and copper losses), as well as the efficiency map.

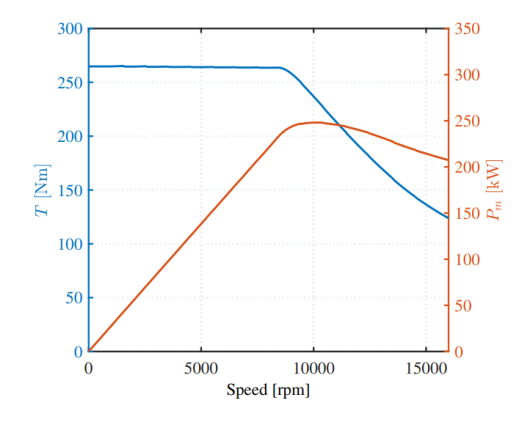


Figure 1.8: Torque and Power curves

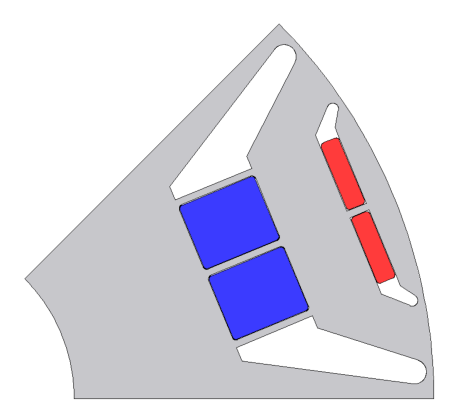


Figure 1.9: Cross-section

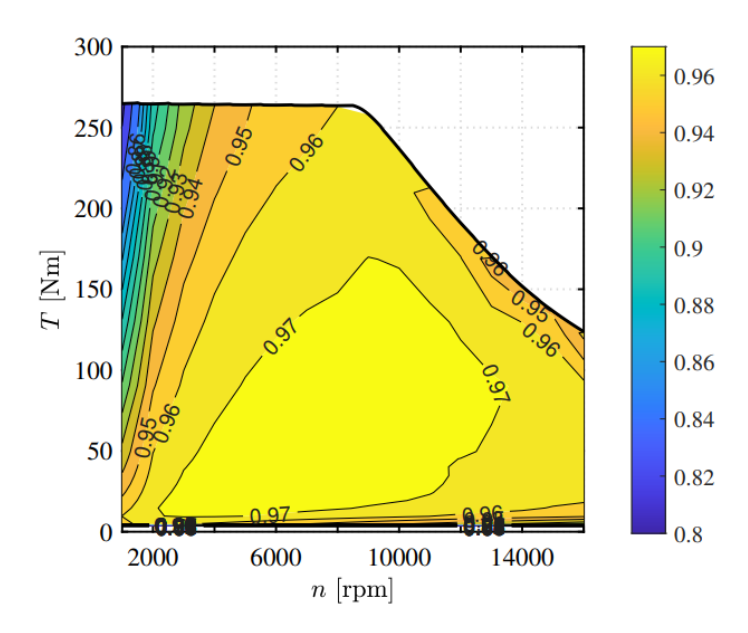


Figure 1.14: Efficiency map

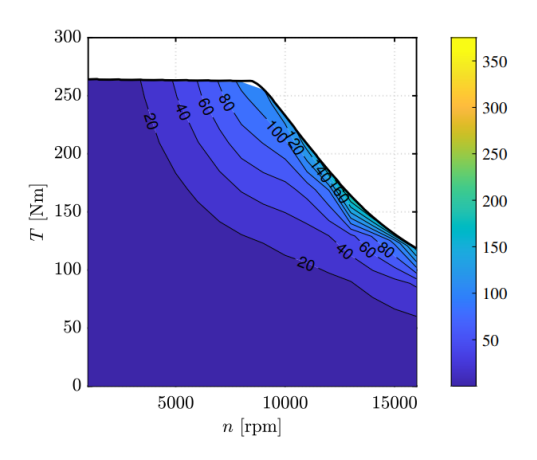


Figure 1.10: PM losses

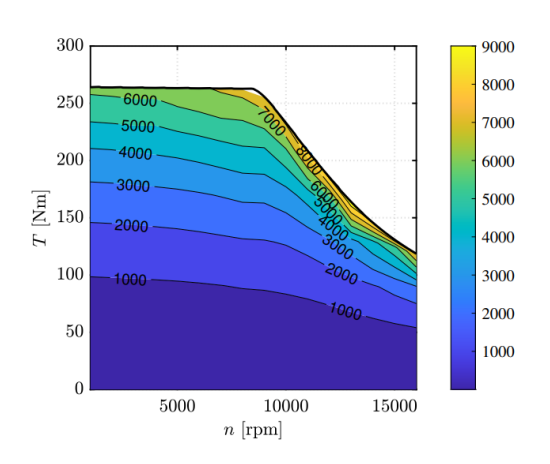


Figure 1.12: Copper losses

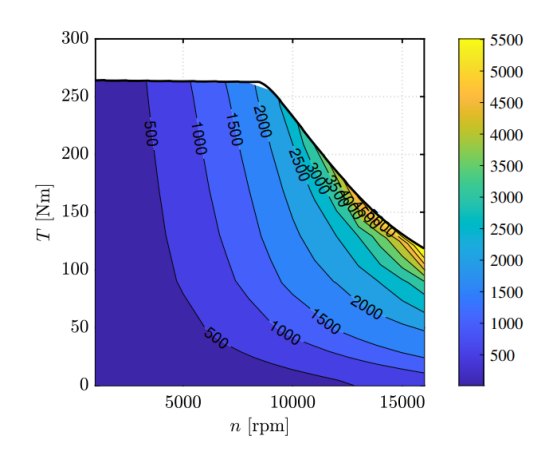


Figure 1.11: Iron losses

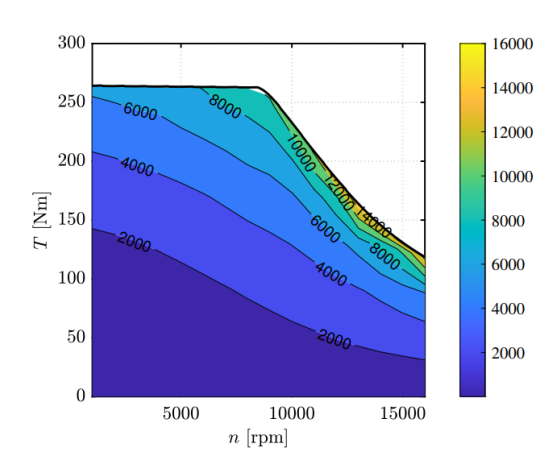


Figure 1.13: Total losses

2 Proposed Design Methodology

2.1 Motor Model

As a starting point, a Surface-mounted Permanent Magnet (SPM) motor was chosen, whose main technical specifications are reported in Table 2.1. The SPM configuration was selected since, as discussed previously, it exhibits the lowest ratio between the remagnetization current and the demagnetization current when compared to alternative rotor topologies, making it particularly suitable for the objectives of this work [6].

Table 2.1: Volvo Cars proprietary SPM motor data

Inner Stator Diameter	154.1 <i>mm</i>
Outer Stator Diameter	$235 \ mm$
Type of Slots	Rectangular
Number of Slots	48
Wire Technology	Hairpin
Number of layers	6
Rotor Diameter	152.2 <i>mm</i>
Shaft Diameter	60~mm

During the design phase, the stator geometry and windings were intentionally kept unchanged. Consequently, the optimization efforts were focused exclusively on the rotor, with modifications to its geometry, dimensions, and magnetic characteristics aimed at enhancing machine performance in line with the project objectives.

Building upon this baseline model, the next step was the modeling and simulation in JMAG, which served to validate the initial configuration and establish the foundation for the subsequent optimization process.

2.2 JMAG Setup

As described earlier, the design and simulation of the motor were carried out using JMAG. The geometric modeling was performed through the integrated Geometry Editor, which allowed the creation of a precise CAD model of the motor fully compliant with the design specifications. Once the geometry definition was completed, a 2D Magnetic Field Transient Analysis was performed to evaluate the electromagnetic behavior of the system.

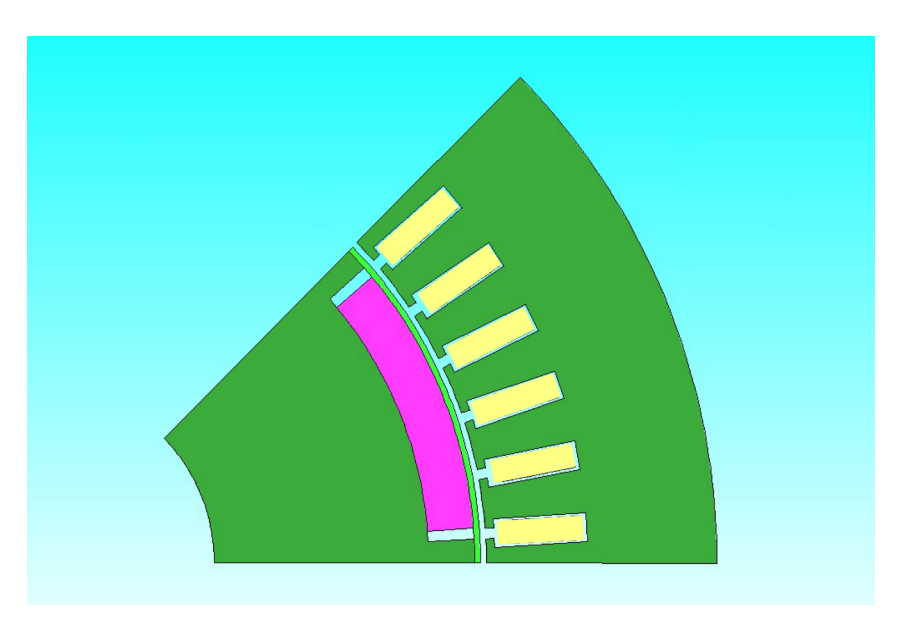


Figure 2.1: Jmag Designer

Before running the simulations, it was necessary to integrate the iron nitride magnetic material, provided by the partner company, into the model. Using the experimental data supplied, the corresponding B-H characteristic was entered into JMAG's built-in Material Editor, selecting the option for nonlinear magnetic behavior (Nonlinear (Irreversible/Thermal Demagnetization/Demagnetizing Field) – Bilinear Approximation, Fig.2.2).



Figure 2.2: Nonlinear magnetic behavior setting

In particular, to accurately reproduce the B-H curve, the following parameters were defined,

as shown in Fig.2.3.

- Coercivity Force (H_c): the field required to reduce the magnetic induction B to zero after saturation.
- Round Radius: a smoothing factor for the curve near the coercivity point, used to realistically reflect the material's behavior.
- Recoil Permeability (μ_{rec}): the slope of the recovery curve following partial demagnetization.
- Remanence (B_r): the residual magnetic induction at H = 0 after full magnetization.
- Intrinsic Coercivity (\mathbf{H}_{ci}): the field required to reduce the internal induction \mathbf{B}_{int} to zero, measured intrinsically.

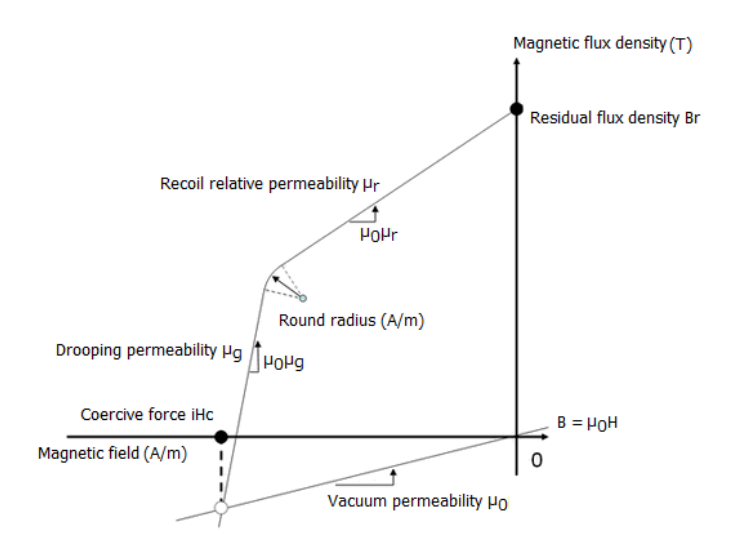


Figure 2.3: Parameters setting

Before proceeding with the actual optimization phase, several preliminary simulations were carried out using different studies to obtain a first qualitative evaluation of the motor's response. Each study was configured to investigate specific aspects of the machine's behavior and required the creation of an equivalent electrical circuit to simulate the power supply conditions during the analysis (Fig.2.4). For each study, multiple simulation cases were implemented to evaluate the performance of the model under different operating conditions and geometric configurations.

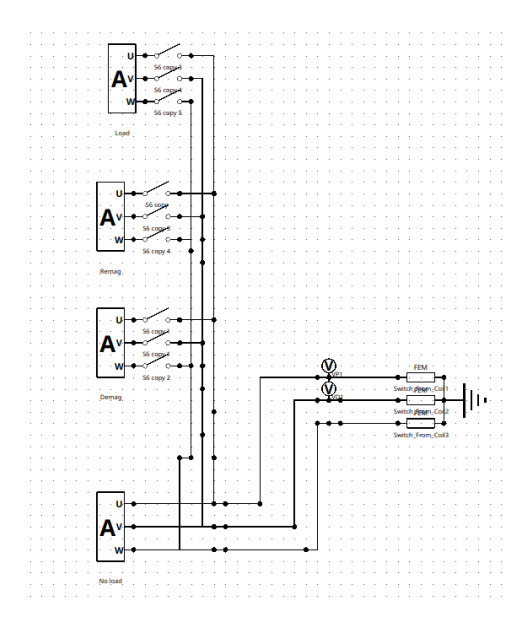


Figure 2.4: Equivalent electrical circuit

Finally, a custom JMAG expression was created to calculate the Magnetization State (MS) defined earlier. This involved computing the initial and final flux over a given period, using only the first harmonic, and then taking their ratio, as illustrated in Figure 2.5.

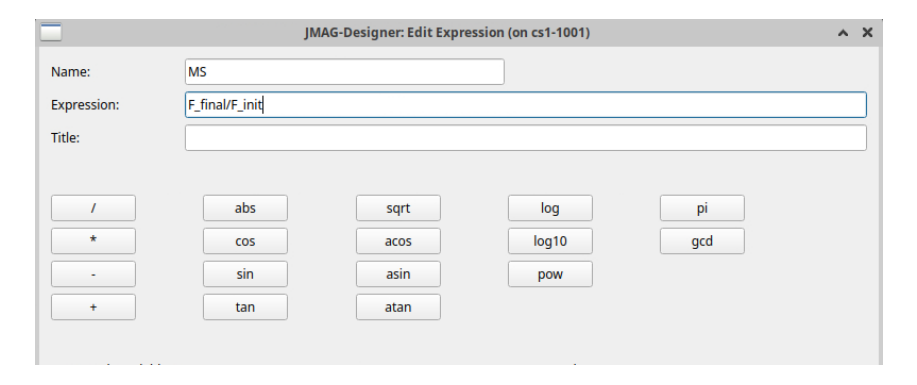


Figure 2.5: MS definition

These steps provided a robust and validated baseline model, setting the stage for the subsequent optimization phase, where the rotor design and control strategies were refined to meet the performance targets of the project.

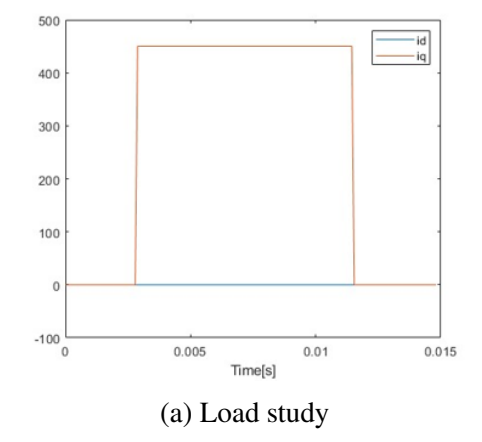
2.3 Optimization First Method

To define the design methodology, a direct optimization-based approach was adopted, implemented with two different optimization configurations.

2.3.1 Study

The first optimization was organized as an Analysis Group consisting of two distinct studies, each aimed at achieving specific objectives.

- *First Study*: This study includes an initial electrical period in no-load, followed by three electrical periods in load (with current injection exclusively along the q-axis), and a final period in no-load. The primary goal of this configuration is to achieve the torque target, optimizing the motor geometry and parameters to ensure the desired torque under the defined operating conditions (Fig.2.6a).
- *Second Study*: The second study begins with a no-load period, followed by two periods with negative d-axis current injection to induce magnet demagnetization. This is followed by three periods in no-load, then two periods with positive d-axis current injection to perform remagnetization of the magnet, and concludes with a final no-load period. The purpose of this configuration is to minimize the remag/demag current ratio, defined as the ratio between the current required to remagnetize the magnet and the current needed to demagnetize it (Fig.2.6b).



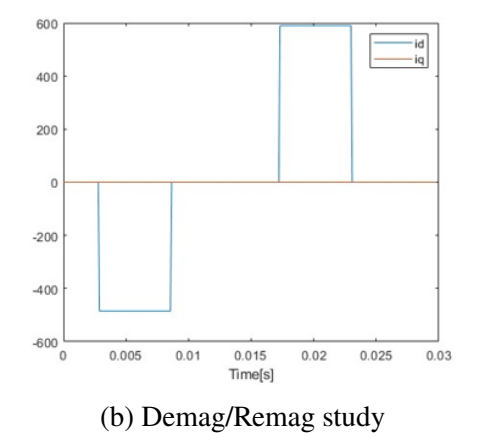


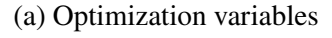
Figure 2.6

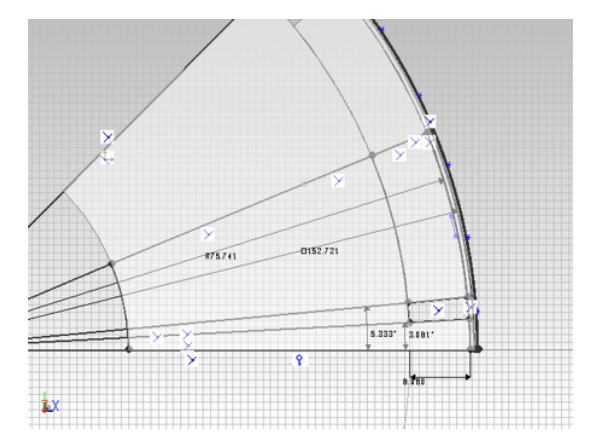
2.3.2 Optimization Setting

For the optimization configuration, the design variables reported in Fig2.7a were selected, each defined within a specific range between a minimum and a maximum value. In particular, the parameters considered include:

- Total machine length;
- Load current;
- Demagnetization current;
- Remagnetization current;
- Magnet dimensions (thickness and lenght);
- Pocket dimensions to accommodate the magnet (thickness and lenght);

Variable	Min	М	ах
Length		139	145.2
I_load		300	777
I_remag		700	3000
angle_start_pocket		1	5
PM_pocket_h		5.1	9
PM_Tichness		5	8.9
Angle_start_PM		1.5	7
I_demag_10		300	500





(b) CAD parameters

Figure 2.7

The objective functions were defined to ensure the required performance targets and the correct magnetic behavior of the system. Specifically:

- Maximum torque: must be greater than 250 Nm;
- After-load Magnetization State (MS): must remain above 80%;
- Remag/Demag current ratio (I_{remag}/I_{demag}): to be minimized, in order to reduce the current required to restore magnetization relative to that needed for demagnetization;

- After-demagnetization MS: should be approximately 10%, with a maximum deviation of $\pm 1\%$;
- After-remagnetization MS: should be approximately 80%, with a maximum deviation of $\pm 1\%$.

A summary of these parameters and objectives is provided in Fig.2.8.

Parameter	Expression	Type		Value	Weight	
MS_after_load	F_final_1/F_init_1	>=	*	0.8	9	
T_load	Torque_LOAD/250	>=	*	1	10	
remag_demag_ratio	I_remag/I_demag_10	Minimize	*		6	
4 MS_demag_10	abs((F_final_1_demag_DEMAG_REMAG/F_init_1_DEMAG_REMAG)-0.1)	<=	*	0.01	8	
MS_remag_80	abs((F_final_1_remag_DEMAG_REMAG/F_init_1_DEMAG_REMAG)-0.8)	<=	٠	0.01	8	

Figure 2.8: Objective functions

From a computational perspective, the problem was formulated as a multi-objective optimization. In this framework, each objective was treated with different levels of importance, while the physical constraints were implemented as hard conditions, meaning that any violation resulted in the exclusion of that design from the feasible population. The optimization algorithm then explored the solution space within the defined limits, seeking the best possible trade-off among the different performance metrics.

The resulting set of solutions formed the basis for the Pareto set analysis, which enabled the identification of optimal designs balancing torque capability and current efficiency.

2.3.3 Pareto Set Analysis

At the end of the optimization phase, the results were processed using a custom Python script developed for the identification of the solutions that belongs to the Pareto Front.

The first step involved a data filtering process, aimed at selecting only those solutions most relevant to the design requirements. This filtering allowed the removal of configurations that did not meet the defined constraints, focusing the analysis on the most promising designs.

Subsequently, the procedure for the Pareto set identification was implemented, with the optimization criteria set to minimize the I_{remag}/I_{demag} ratio and maximize the Magnetization State after load (MS after load).

From a theoretical perspective, a Pareto-optimal solution is defined as a configuration for which no other solution exists that simultaneously improves all the considered objectives. In other words, moving from one Pareto-optimal solution to another requires accepting a trade-off, improving one performance metric at the expense of another. This concept is particularly relevant in multi-objective optimization problems, as it enables the identification of a set of solutions that are equally optimal, leaving the final choice to the designer based on priorities or application-specific constraints.

In Fig.2.9, all filtered solutions are shown in blue, while the Pareto-optimal solutions are highlighted in orange. These represent the best trade-offs between the considered metrics, as no other configuration can simultaneously improve both objectives without compromising the other.

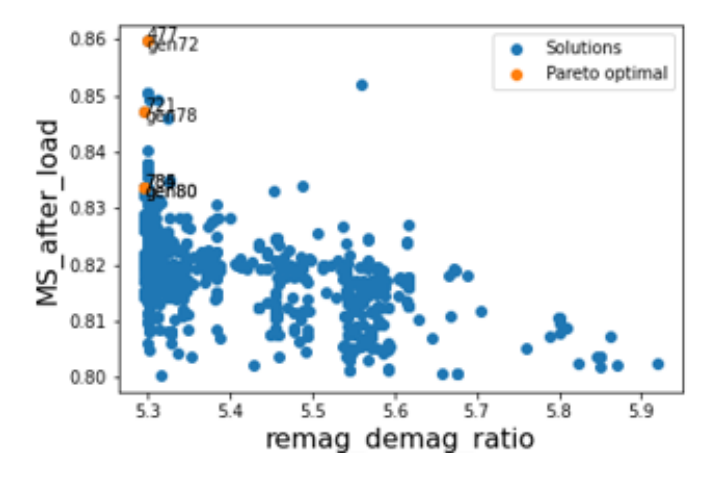


Figure 2.9: Pareto front

2.3.4 Results

The analysis led to the identification of four distinct solutions, summarized in Fig2.10., where the corresponding values of the design variables are reported. The configuration providing the best overall performance was selected as the final design, and its geometry is illustrated in Fig.2.11.

Case	MS_after_load	T_load	remag_demag_rati	MS_demag_10	MS_remag_	Torque_LOAD	Length	I_remag	angle_start_pock	PM_pocket_h	PM_Tichness	R_end_PM	Angle_start_PM	l_demag_10	I_load
477	0.86	1.00	5.30	0.009	0.009	250.6	144.86	1981.9	1.18	8.18	8.14	76.22	4.14	374.0	437.7
721	0.85	1.01	5.30	0.010	0.010	252.7	144.97	1981.9	1.24	8.18	8.14	76.22	4.13	374.2	468.1
784	0.83	1.01	5.30	0.010	0.010	251.4	143.23	1981.9	1.24	8.18	8.14	76.22	4.14	374.2	501.6
785	0.83	1.02	5.30	0.010	0.010	254.7	145.15	1981.9	1.23	8.18	8.14	76.22	4.14	374.2	501.6

Figure 2.10: Best design solutions

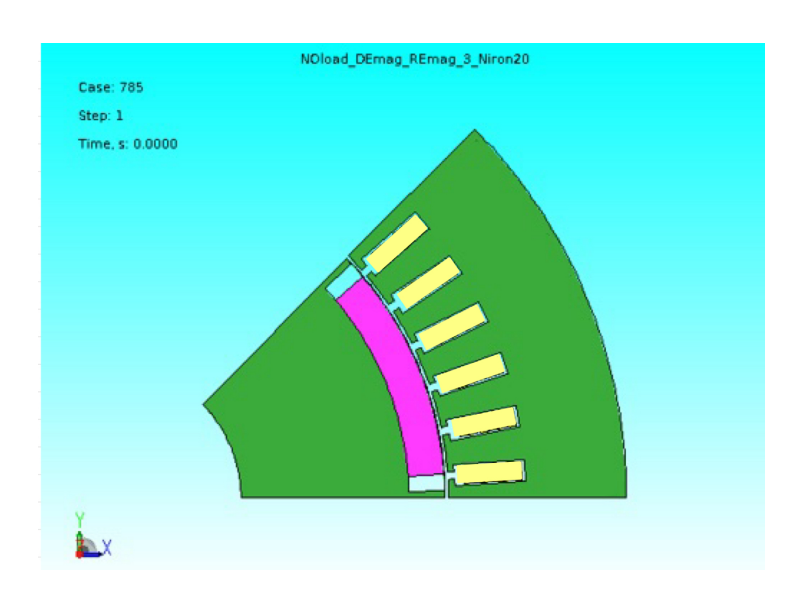


Figure 2.11: Motor model

Fig.2.12 shows the terminal voltage profile during the test cycle. It can be observed that the magnet was demagnetized until the Magnetization State (MS) reached 10%, then remagnetized up to 80%, and finally subjected to the load application. However, after the load step, both the voltage waveform and the MS value appear different compared to the pre-load conditions.

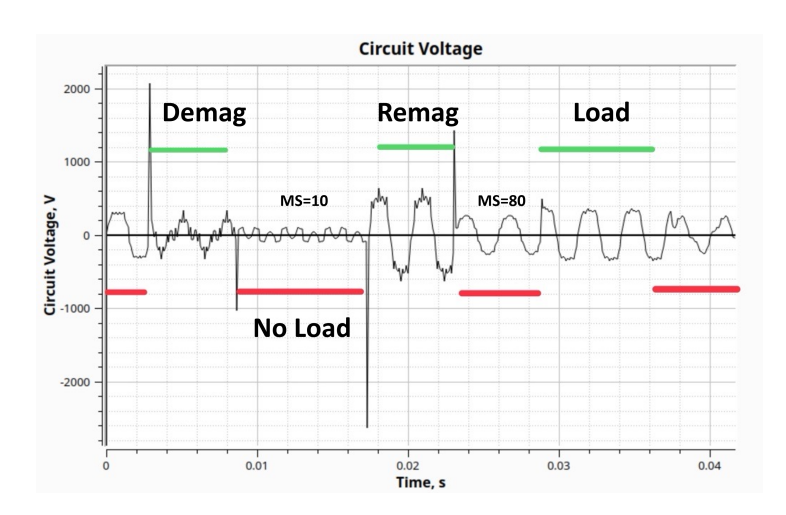


Figure 2.12: Circuit voltage profile

The electromagnetic torque profile, shown in Fig.2.13, further highlights this behavior: the achieved torque value did not reach the target of 250 Nm, falling slightly below the desired specification.

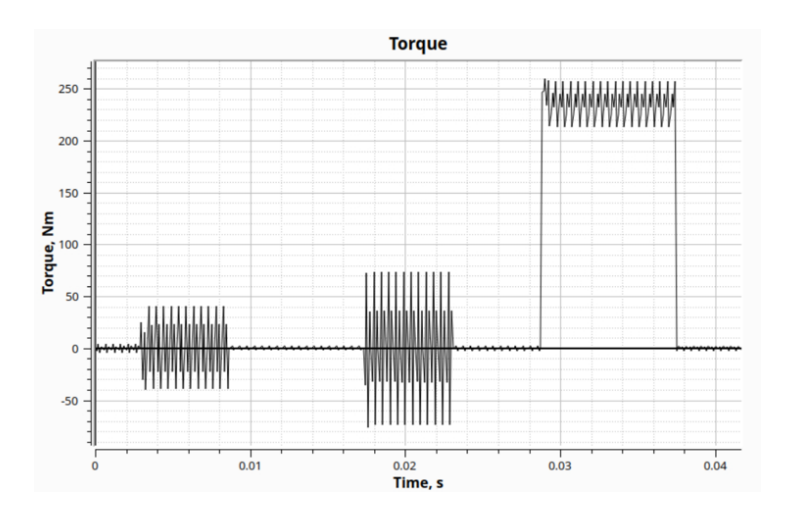


Figure 2.13: Torque profile

Although this first optimization phase did not fully meet the torque requirement, it provided valuable insights into the machine's magnetic and dynamic behavior, serving as a solid baseline for refining the design approach. Building on these results, a second optimization phase — described in the following section — was carried out, introducing targeted adjustments to both the design parameters and the optimization strategy, with the goal of increasing torque while preserving the desired magnetic performance and overall system stability.

2.4 Optimization Second Method

The second optimization phase was developed to overcome the limitations observed in Optimization 1, particularly the inability to achieve the target torque of 250 Nm and the undesired variations in the Magnetization State (MS) after load application. The primary objective of this new strategy was to simplify the simulation process and expand the design space, while keeping the key constraints on the magnetic behavior unchanged.

2.4.1 Study

Unlike the previous approach, Optimization 2 employs a single study in which the three phases, demagnetization (demag), remagnetization (remag), and load, are integrated into one continuous time sequence. The simulation begins with a no-load period, followed by two demagnetization periods with negative d-axis current, then three additional no-load periods. This is followed by two remagnetization periods with positive d-axis current, another sequence of three no-load periods, and finally three load periods with q-axis current before concluding with two final no-load periods (Fig.2.14).

This continuous-cycle setup makes it possible to analyze the entire operating behavior of the motor within a single simulation, significantly reducing computational time and ensuring greater consistency across the different phases. These improvements provided a more robust foundation for the optimization process, whose results and performance assessment are discussed in the following sections.

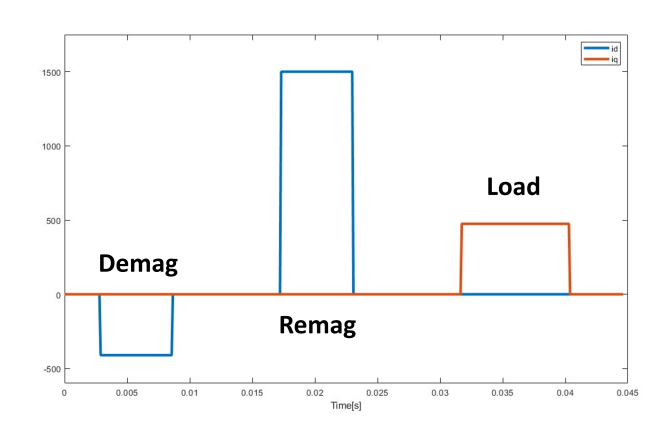


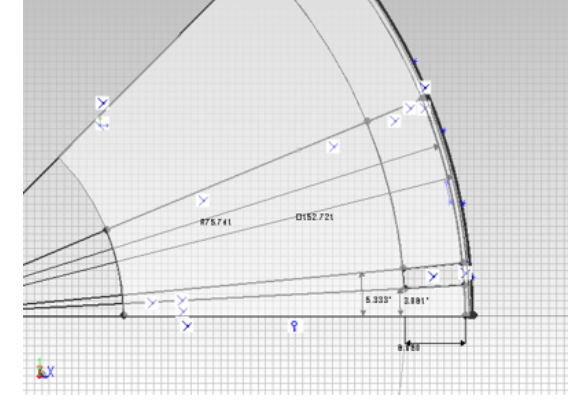
Figure 2.14: Study profile

2.4.2 Optimization Setting

As in the previous method, a set of design variables was defined, but with some significant modifications:

- **Rotor diameter** (new variable);
- Total machine length (range adjusted to 150-170 mm);
- Load current;
- Demagnetization current;
- Remagnetization current;
- Magnet dimensions (thickness and lenght);

Variable	Min	1	Max
Length		139	145.2
I_load		300	777
I_remag		700	3000
angle_start_pocket		1	5
PM_pocket_h		5.1	9
PM_Tichness		5	8.9
Angle_start_PM		1.5	7
I_demag_10		300	500



(a) Optimization variables

(b) CAD parameters

Figure 2.15

The objective functions remained essentially the same as in the first optimization, with one key difference: the torque constraint was relaxed, requiring a minimum torque of 230 Nm instead of 250 Nm. This adjustment aimed to increase the number of feasible solutions and provide greater flexibility in finding an optimal trade-off between performance metrics.

The optimization objectives were defined as follows:

- Maximum torque: must be greater than 230 Nm;
- After-load Magnetization State (MS): must remain above 80%;

- Remag/Demag current ratio (I_{remag}/I_{demag}): to be minimized, in order to reduce the current required to restore magnetization relative to that needed for demagnetization;
- **After-demagnetization MS**: should be approximately 10%, with a maximum deviation of ±1%;
- After-remagnetization MS: should be approximately 80%, with a maximum deviation of $\pm 1\%$.

A summary of the design variables and objective functions is provided in Fig.2.15a and Fig.2.16.



Figure 2.16: Objective functions

These configurations set the stage for the Pareto set analysis, enabling the identification of optimal solutions that balance torque performance, current efficiency, and magnetic stability.

2.4.3 Pareto Set Analysis

As in the first optimization phase, the results of Optimization 2 were processed using a custom Python script developed for the generation of the Pareto Set Machine.

The procedure consisted of two main steps:

- 1. **Data filtering**: Only the solutions fully compliant with the design constraints were selected, narrowing the analysis to the most promising configurations.
- 2. **Definition of optimization criteria**: As in the previous phase, the analysis was performed by imposing the minimization of the I_{remag}/I_{demag} ratio and the maximization of the Magnetization State after load (MS after load).

In Fig.2.17, all the filtered solutions are shown in blue, while the Pareto-optimal solutions are highlighted in orange. These represent the best trade-offs between the considered metrics and therefore served as the foundation for selecting the final configuration.

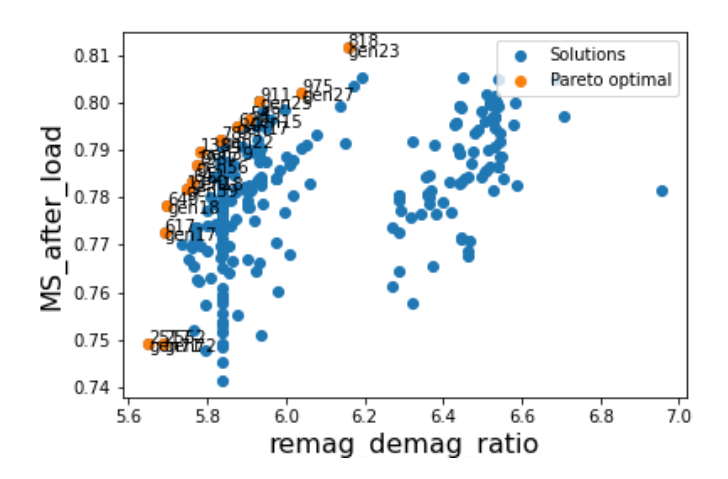


Figure 2.17: Pareto front

Building on this analysis, the next step focused on a detailed evaluation of the selected optimal solutions, whose performance and design characteristics are discussed in the following section.

2.4.4 Results

The optimization conducted with the second method yielded a larger number of valid solutions compared to the previous phase. All the configurations obtained, along with the corresponding values of the design variables, are summarized in Fig.2.18.

Case	MS_after_load <u>*</u>	Ratio Demag/Remag 💌	Torque_load 💌	MS_remag <u></u>	MS_demag <u></u>	Lenght 💌	Rotor_r 💌	I_remag <u></u>	I_demag_10 <u></u>	I_load
549	0.80	5.9	231	0.83	0.05	160	168	2449	415	325
617	7 0.77	5.7	231	0.82	0.08	159	168	2367	416	335
629	0.80	5.9	230	0.83	0.06	160	168	2449	417	325
640	0.78	5.7	231	0.82	0.10	160	168	2400	421	325
642	0.78	5.8	233	0.82	0.10	160	168	2427	421	332
783	0.79	5.8	232	0.83	0.10	160	168	2456	421	325
818	0.81	6.2	231	0.85	0.07	158	168	2550	414	321
911	1 0.80	5.9	231	0.83	0.07	159	168	2456	414	321
975	0.80	6.0	232	0.84	0.08	159	168	2501	414	321
1384	1 0.79	5.8	230	0.83	0.08	159	168	2404	416	322
1390	0.78	5.7	230	0.82	0.09	160	168	2401	418	325
1987	7 0.79	5.8	230	0.82	0.09	159	168	2427	420	325
2517	7 0.75	5.7	235	0.81	0.11	155	165	2427	429	341
2552	0.75	5.7	235	0.81	0.10	155	165	2427	426	341

Figure 2.18: Best design solutions

For a more targeted analysis, three representative configurations were selected:

- 1. the first, characterized by the **highest Magnetization State (MS)**;
- 2. the second, corresponding to the **lowest** I_{remag}/I_{demag} **ratio**;
- 3. the third, chosen as an **intermediate solution**, providing a balanced trade-off between the two criteria.

The main values related to these three configurations are summarized in Fig.2.19, while a graphical representation of the optimized geometry is shown in Fig.2.20.

Case	2517	818	1987
LENGHT (mm)	155	158	159
STATOR_DIAM (mm)	235	235	235
ROTOR_DIAM (mm)	155	168	168
I_LOAD_peak (A)	341	321	325
TORQUE (Nm)	<mark>235</mark>	<mark>231</mark>	<mark>230</mark>
I_DEMAG_10 (A)	429	414	420
I_REMAG_80 (A)	2427	2550	2427

Figure 2.19: Three best cases

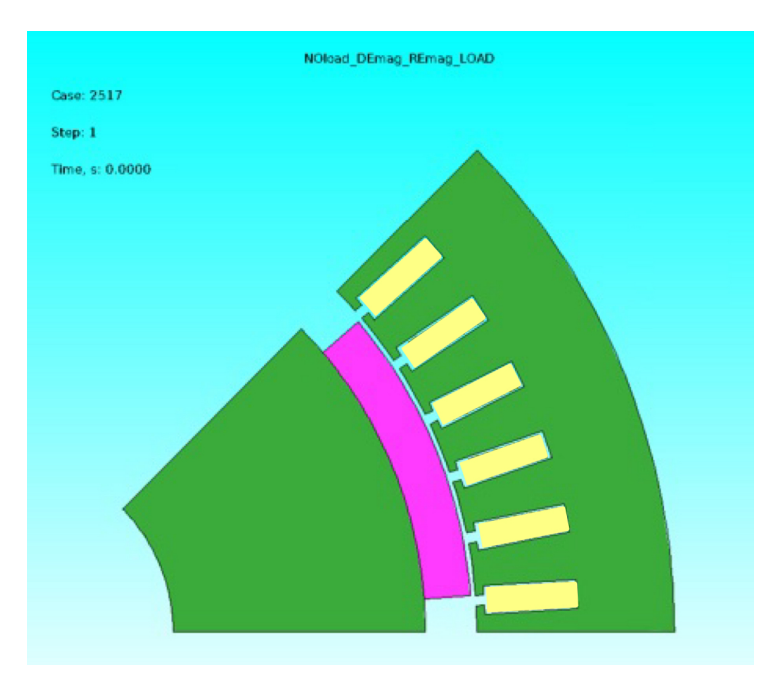


Figure 2.20: Geometry of case 2517

From an electrical standpoint, the analysis of the new circuit voltage waveform revealed a particularly significant improvement: the after-load voltage profile closely matches the pre-load waveform, indicating enhanced operational stability compared to the previous optimization. Furthermore, the Magnetization State successfully reached the target value of 80%, confirming the effectiveness of the method and the validity of the identified solutions (Fig.2.21).

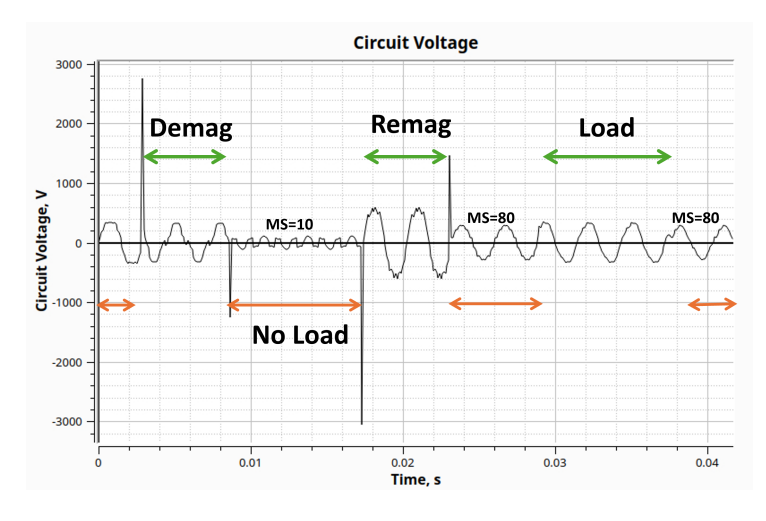


Figure 2.21: Circuit voltage profile

2.4.5 Selection of the Final Solution

Among the three configurations selected from the Pareto front, it was necessary to identify a final solution to be adopted as the reference for the validation phase. The choice was guided by a comparative assessment based on two main criteria:

- 1. **The Magnetization State (MS) after load close to 80%**, a key condition to ensure the proper functionality of the machine in real-world applications.
- 2. Efficiency of the remagnetization process, expressed by the I_{remag}/I_{demag} ratio, which should be kept as low as possible to minimize the energy impact of the operation.

Based on these considerations, the case 2517 was identified as the most balanced option. While it does not achieve the absolute best result in any single parameter, it offers an effective compromise between the two performance metrics, maintaining the post-load MS close to 80% while ensuring a sufficiently low I_{remag}/I_{demag} ratio. This configuration was therefore selected as the final design for subsequent in-depth analyses and validation activities.

2.5 Reuse Demagnetization condition

During the simulation activities, an additional JMAG feature was identified that proved particularly useful for optimizing computation time, known as Reuse Demagnetization. This option allows the magnetization state calculated in a previous study to be used as the initial condition for a subsequent study, thereby avoiding the need to repeat the demagnetization phase in every analysis (Fig.2.22).

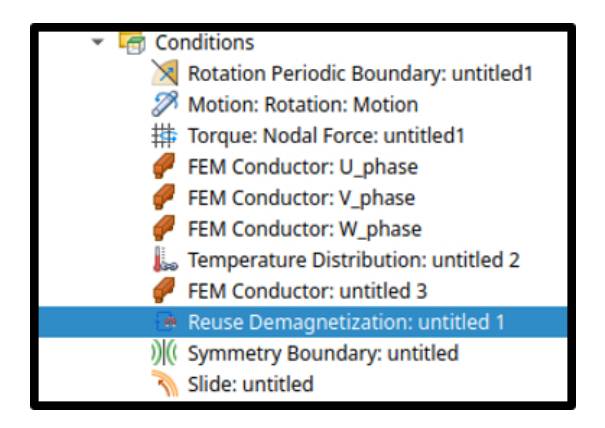


Figure 2.22: Reuse demagnetization condition

For example, in cases where two separate studies are defined, the first can be used to perform the demagnetization of the magnet, and the resulting magnetization state can then be imported into the second study, which may focus on different operating conditions. The only requirement is to properly configure the second study to reference the magnetic result from the first one (Fig.2.23).

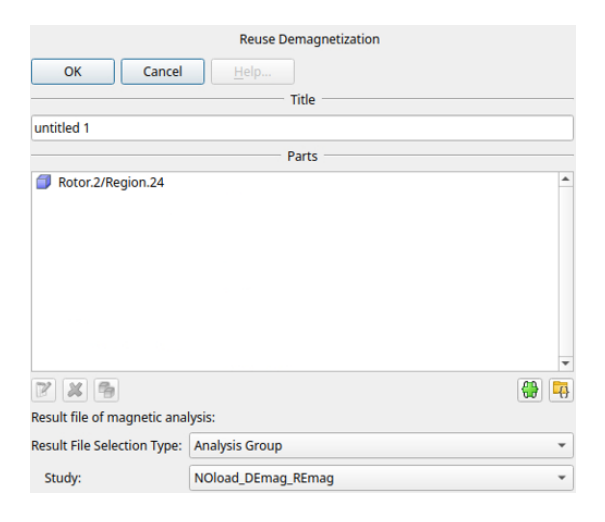


Figure 2.23: Condition Setting

To validate the effectiveness of this feature, a direct comparison was performed between two simulations:

- one implemented as a **single study**, containing the full demagnetization—remagnetization—load sequence (Fig.2.26a);
- one structured as an **analysis group**, where the demagnetization and remagnetization phases were separated from the load phase, using the Reuse Demagnetization option to transfer the magnetic state from the first study to the second (Fig.2.26b).

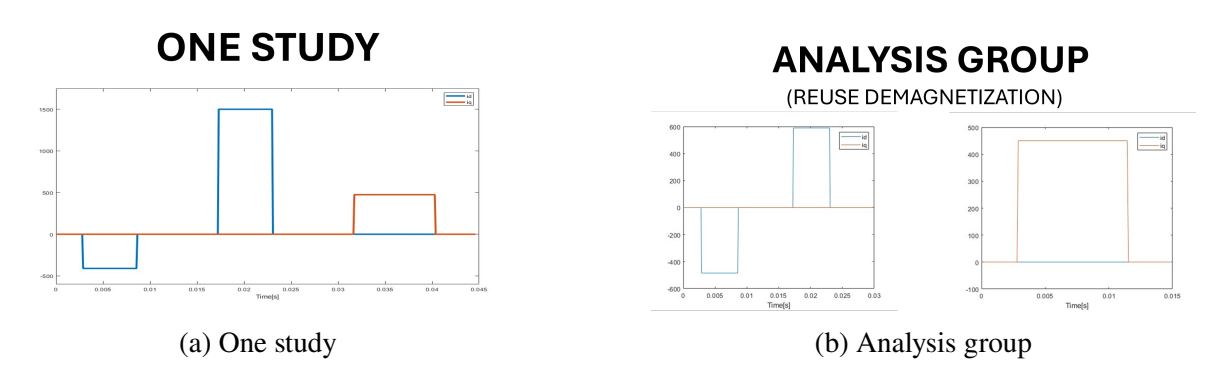
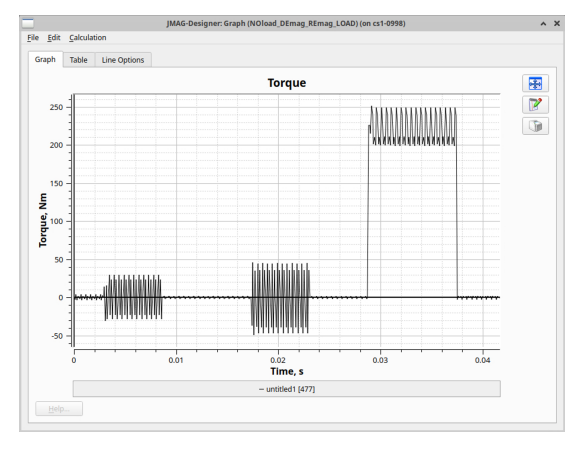


Figure 2.24: Study definition

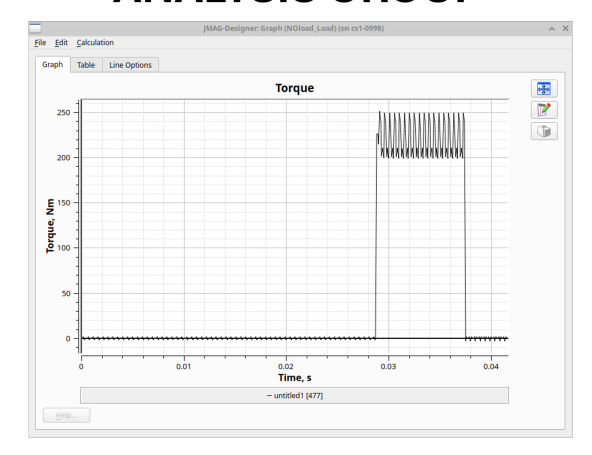
The results showed an almost perfect overlap between the two approaches: both the torque waveform during the load period (Fig.2.25) and the circuit voltage profile (Fig.2.26) matched with high accuracy. This confirms that the Reuse Demagnetization feature can be safely used, providing a significant reduction in simulation time without compromising the accuracy or reliability of the results.

ONE STUDY



(a) One study

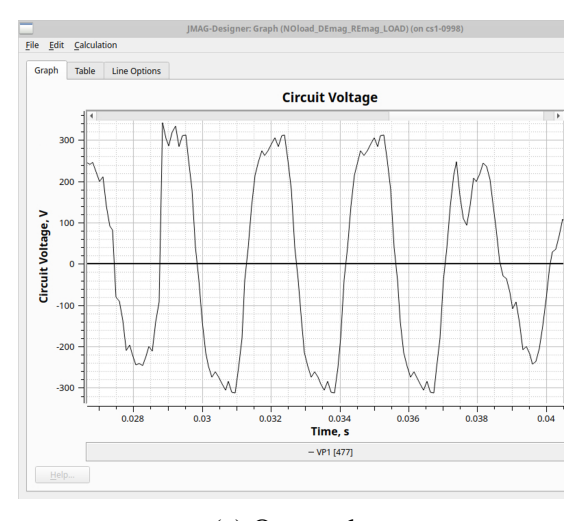
ANALYSIS GROUP



(b) Analysis group

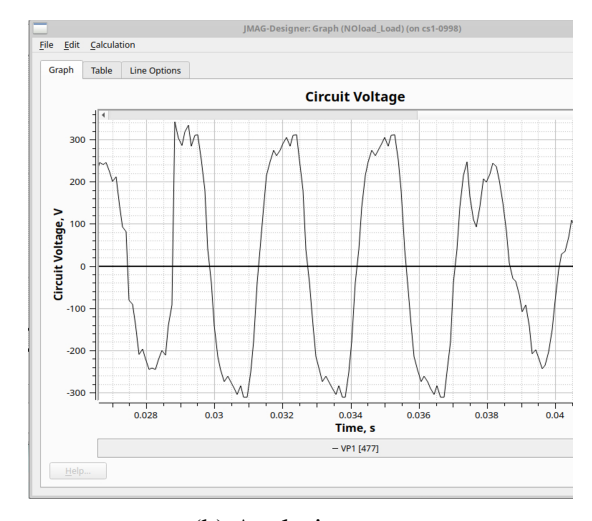
Figure 2.25: Torque profile

ONE STUDY



(a) One study

ANALYSIS GROUP



(b) Analysis group

Figure 2.26: Circuit voltage profile

2.6 Conclusion

This chapter has described the workflow adopted for the modeling, simulation, and optimization of the Variable Flux Machine (VFM) using the JMAG software. After outlining the preliminary model setup, including the integration of iron nitride magnetic material with its nonlinear properties, the process moved on to the configuration of the analyses and the definition of the key design variables.

The first optimization phase, based on a multi-study approach, provided valuable insights into the machine's behavior during demagnetization, remagnetization, and load conditions, while also highlighting certain limitations, such as the difficulty in achieving the target torque. The Pareto front analysis identified a set of optimal solutions, from which the most balanced configuration was selected.

The second optimization phase introduced a more integrated and flexible setup, with an expanded design range and a slightly relaxed torque constraint. This strategy enabled the identification of a larger number of feasible solutions and, in particular, the selection of a configuration that offered a better balance between torque and a reduced remagnetization/demagnetization current ratio.

Finally, the implementation of the Reuse Demagnetization feature demonstrated the potential for further reducing computation times by allowing the reuse of the magnetic state across multiple studies, without compromising the accuracy of the results. This functionality proves to be particularly promising for future large-scale optimization campaigns, making simulations more efficient and scalable.

In summary, the activities described in this chapter not only validated the proposed design and simulation methodology for the VFM but also identified strategies to enhance the overall efficiency of the optimization process. The next chapter will build upon these results, focusing on the detailed analysis of the optimized VFM to validate its behavior and performance across various operating conditions.

3 Motor Analysis

In this chapter, the motor model obtained from the previous optimization process is analyzed using the SyR-e software.

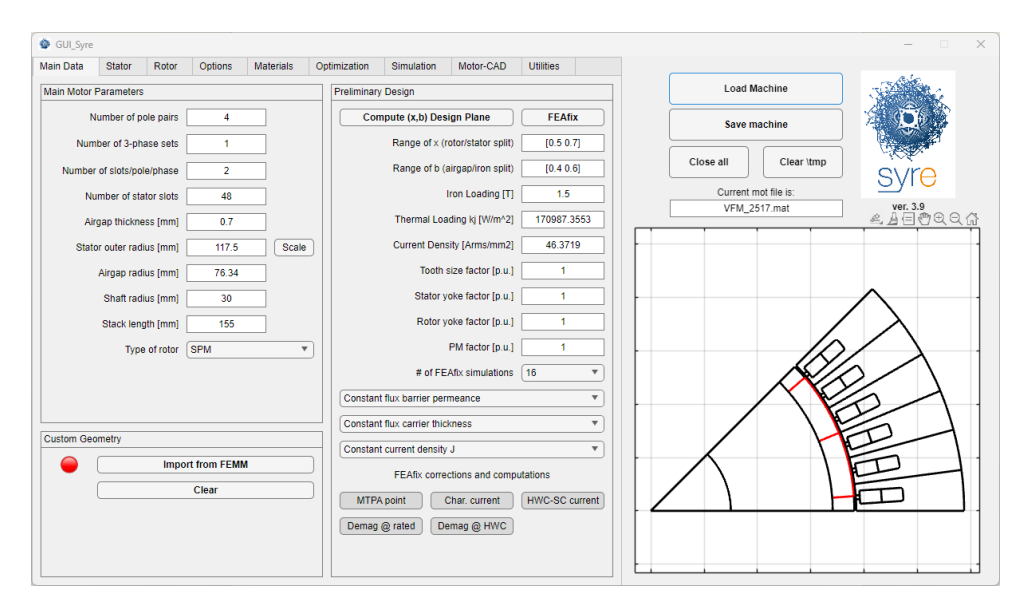


Figure 3.1: Syr-e interface

Since SyR-e requires a specific structure to process models, it was necessary to rebuild the geometry by inputting into the software all the parameters derived from the model developed in JMAG. To ensure compatibility between the two environments, the model had to comply with predefined conventions regarding nomenclature, boundary conditions, and the definition of circuits and studies. Once adapted to these requirements, SyR-e was able to automatically generate a JMAG model ready for analysis.[9]

The outcome of this reconstruction is shown in Fig.3.2. From this model, it was then possible to proceed with the generation of the demagnetization and remagnetization maps. The only element that had to be added manually was the set of hairpins, which are not handled directly by the software.

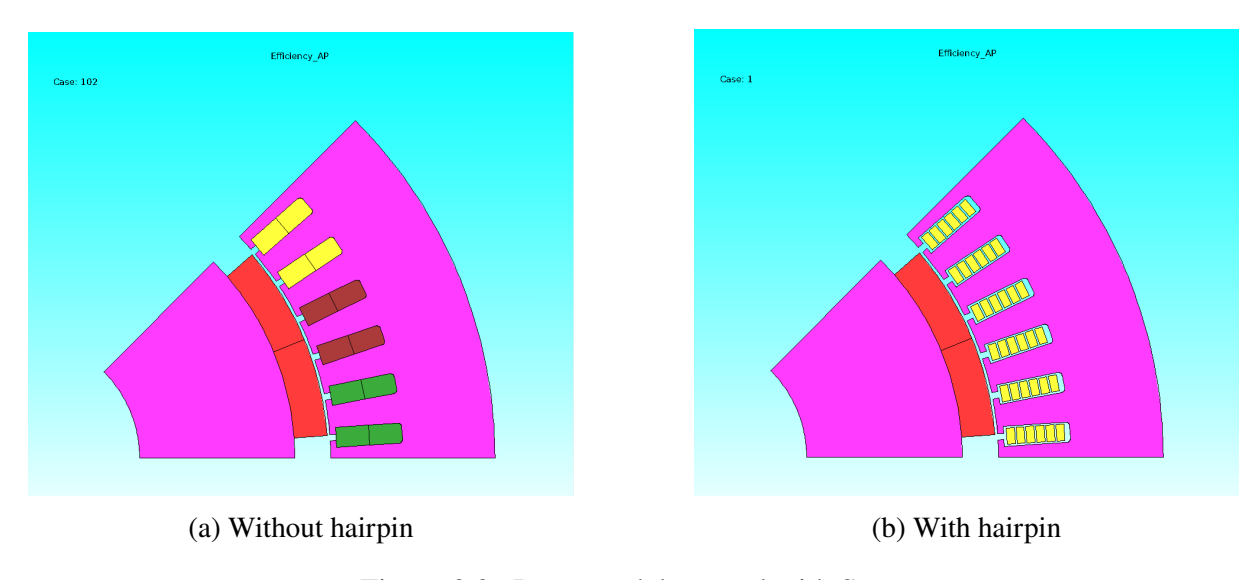


Figure 3.2: Jmag model created with Syr-e

3.1 Demagnetization/Remagnetization Maps

The demagnetization and remagnetization maps represent the amount of i_d and i_q current required to either demagnetize or remagnetize the magnet. These maps illustrate the magnet's response to current excitation, expressing the Magnetization State (MS) as the ratio between the instantaneous magnetic flux and the initial flux (100% MS).

The maps were generated using SyR-e, by setting appropriate current ranges and grid resolutions for the calculations.

- For the demagnetization map (Fig.3.3), the i_d current was varied from -350 A to 0 A, while i_q was swept from 0 A to 400 A, with a grid resolution of 11×11 points.
- For the remagnetization map (Fig. 3.4), the i_d current range was extended from 0 A to 3000 A, while i_q remained in the range of 0 A to 400 A, with a finer grid resolution of 20×20 points.

As expected, the currents required for remagnetization are significantly higher than those needed for demagnetization, in some cases up to ten times greater. These maps are therefore a fundamental tool for determining the currents necessary to adjust the MS of the machine under different operating conditions. They also provide essential insights for defining the motor's control strategy and ensuring optimal flux regulation.

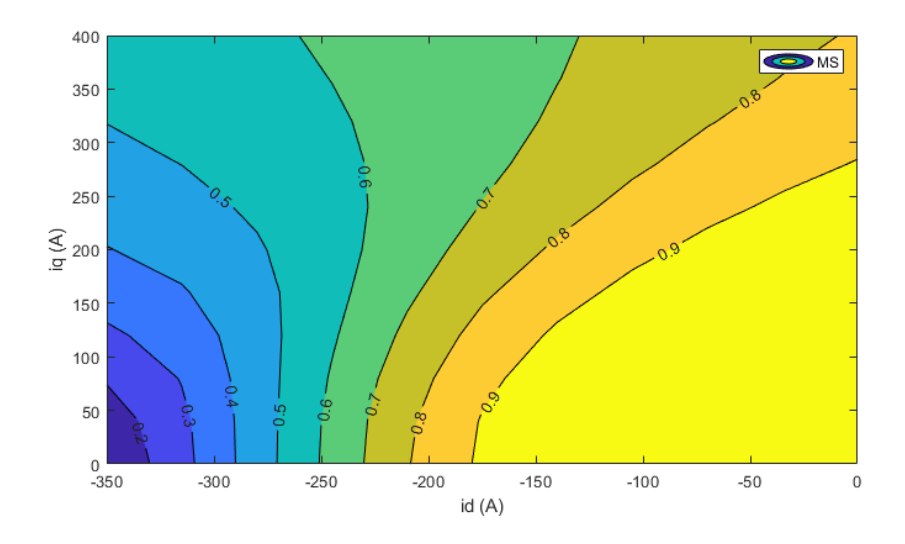


Figure 3.3: Demagnetization map

36

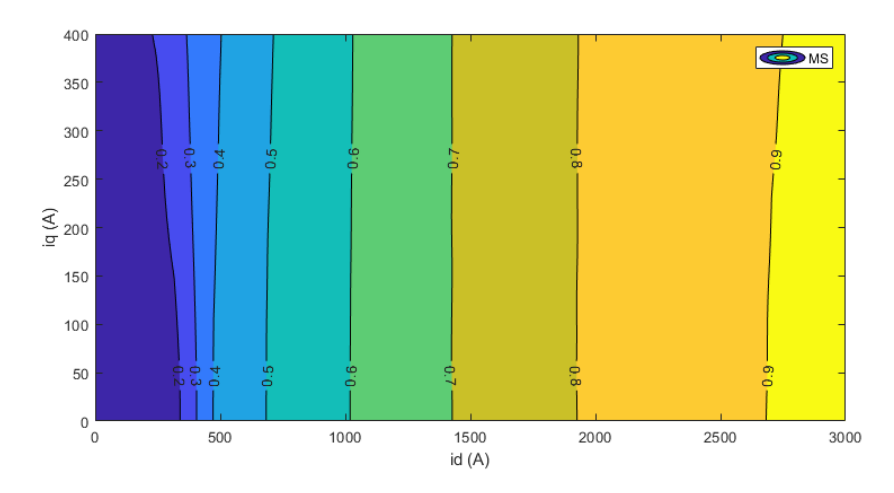


Figure 3.4: Remagnetization map

For example, consider a machine operating at MS = 80%. If currents of $\mathbf{i}_d = -300$ A and $\mathbf{i}_q = 300$ A are applied, the machine would demagnetize to an MS of approximately 50%. To return to the initial state (MS = 80%) while maintaining the same \mathbf{i}_q , a \mathbf{i}_d current of approximately 2000 A would be required, a clear indication of the much higher effort needed for remagnetization compared to demagnetization.

These maps provided the foundation for the subsequent analyses, enabling the generation of flux maps and torque curves across different magnetization states. Such analyses are essential for understanding the electromagnetic behavior of the machine and for evaluating its performance under varying operating conditions.

3.2 Flux maps and Torque curve

Following the generation of the demagnetization/remagnetization maps, the next step in the motor analysis involved the computation of flux maps and torque curves as a function of the Magnetization State (MS), considering values ranging from 40% to 80%. These analyses are crucial to understanding how variations in magnet magnetization affect the overall performance of the machine.

The flux maps (Fig.3.5 and Fig.3.6) describe the distribution of the magnetic flux within the machine as a function of the axial currents i_d and i_q and the current MS level. Due to magnetic saturation and cross-saturation phenomena, the relationship between flux, currents, and magnetization is nonlinear. This nonlinearity implies that small current variations in certain operating regions can lead to very different flux responses depending on the MS level, making the use of an accurate numerical model indispensable. For this reason, the flux maps were generated using SyR-e, which allows the nonlinear effects to be properly captured and enables a detailed analysis of the machine's magnetic response.

It can also be observed that each MS level is associated with a specific current range. Exceeding this range would inevitably drive the machine into either further demagnetization or remagnetization, thus shifting the magnetization state to the adjacent MS level depending on which limit is crossed.

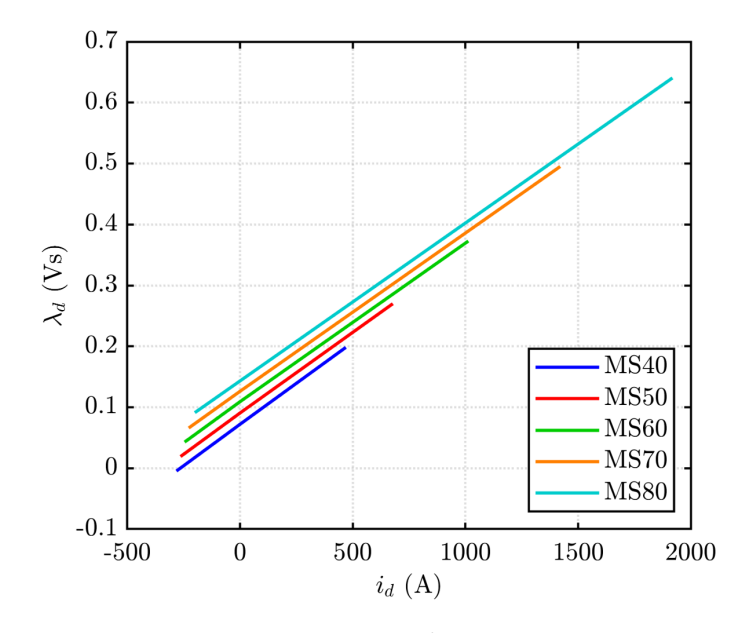


Figure 3.5: Flux map λ_d , i_d with $i_q = 0$

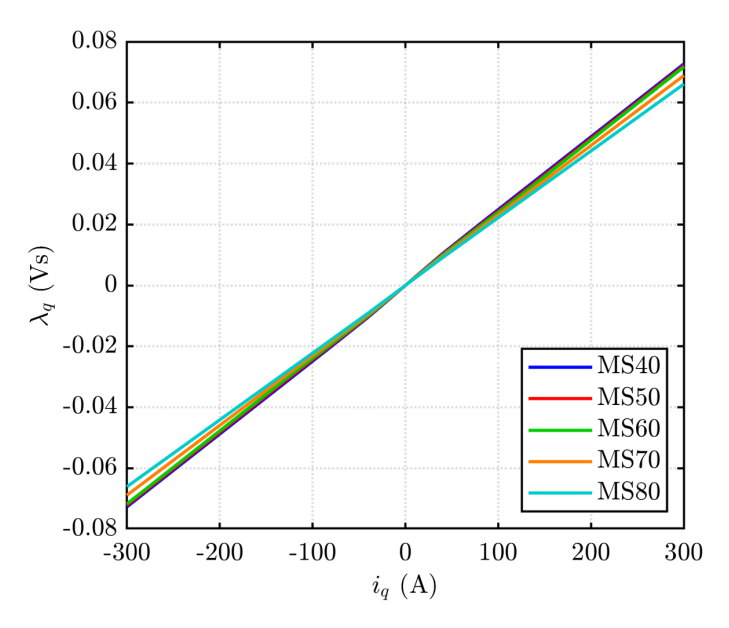


Figure 3.6: Flux map λ_q , i_q with $i_d = 0$

The torque curves (Fig.3.7), also obtained using SyR-e, confirmed the typical behavior of Variable Flux Machines (VFM): as the machine becomes more demagnetized, the maximum available torque decreases, while the operating speed range expands. This result highlights the intrinsic trade-off between torque performance and flux modulation capability that characterizes this class of machines.

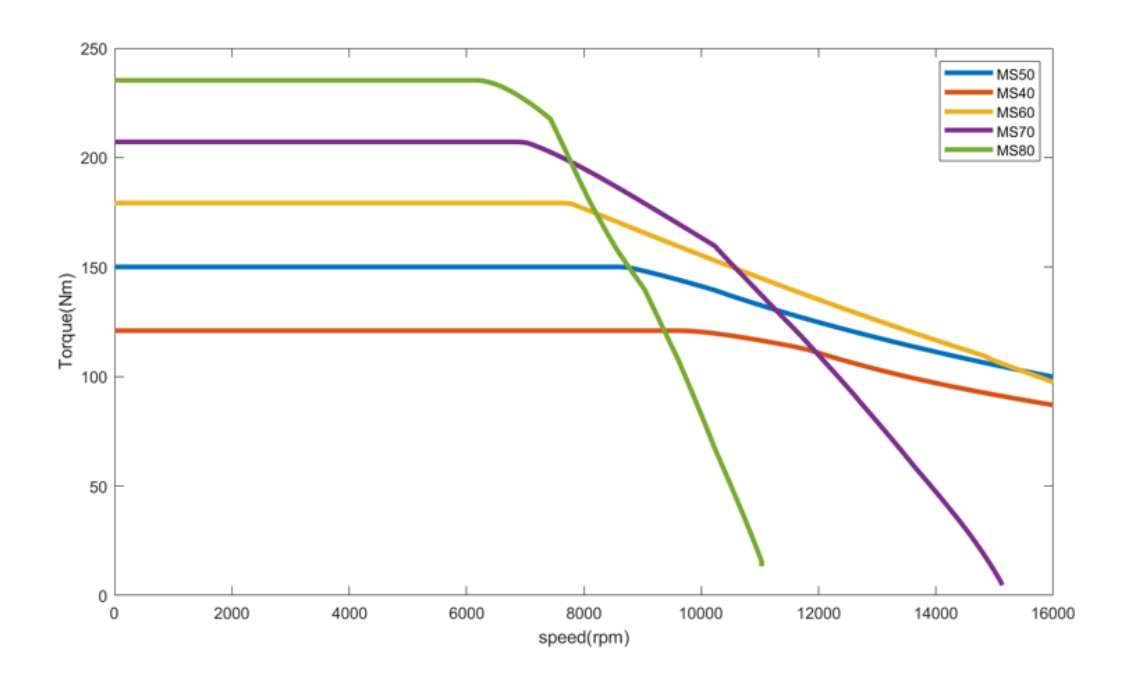


Figure 3.7: T - n curve

To complete the analysis, iso-torque curves were generated for each MS level (Fig.3.8, Fig.3.9 and Fig.3.10). These curves represent the torque behavior as a function of i_d and i_q currents and provide valuable insights for identifying the optimal current combinations required to maintain constant torque. Such information is essential for defining the motor control strategy and for optimizing overall performance across different magnetization states.

In this case as well, the current limits discussed earlier for the flux maps can be clearly observed. They appear as white areas in the plots, corresponding to regions where no feasible values exist since exceeding those limits would shift the machine into a different MS level through either demagnetization or remagnetization.

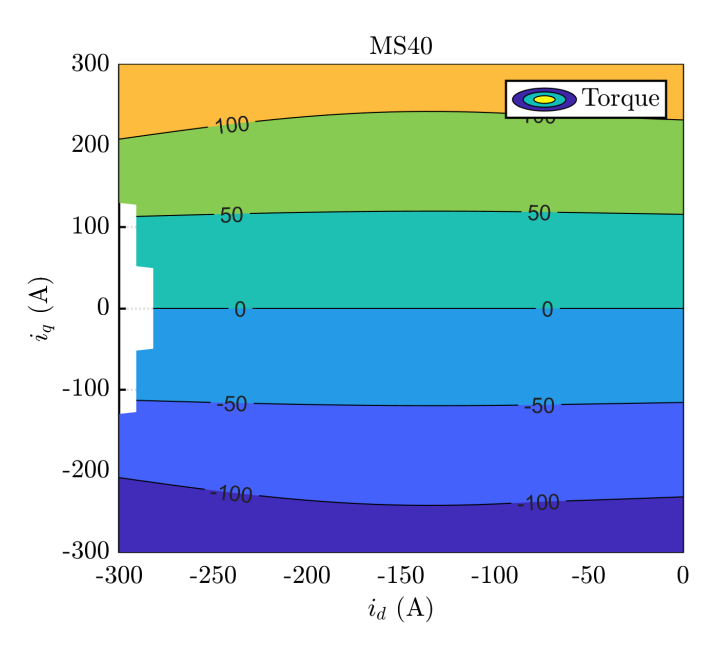


Figure 3.8: Iso-torque for MS40

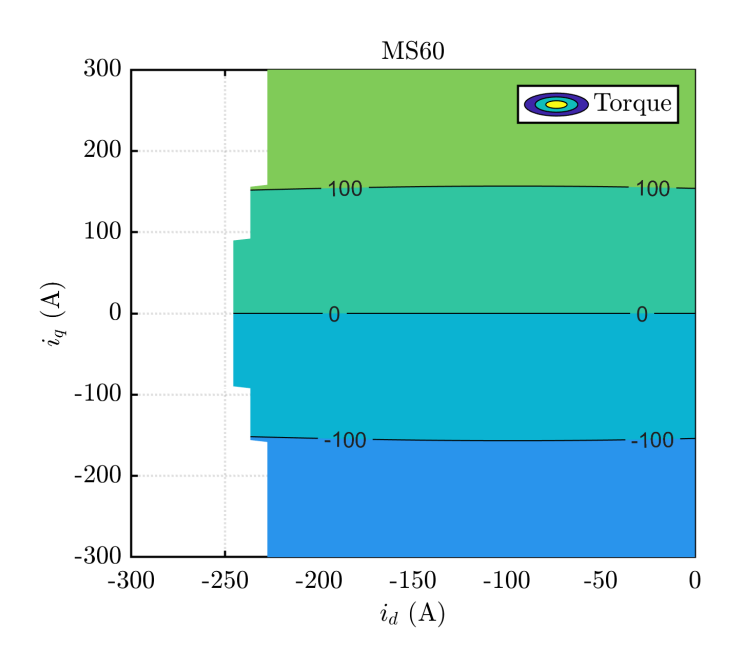


Figure 3.9: Iso-torque for MS60

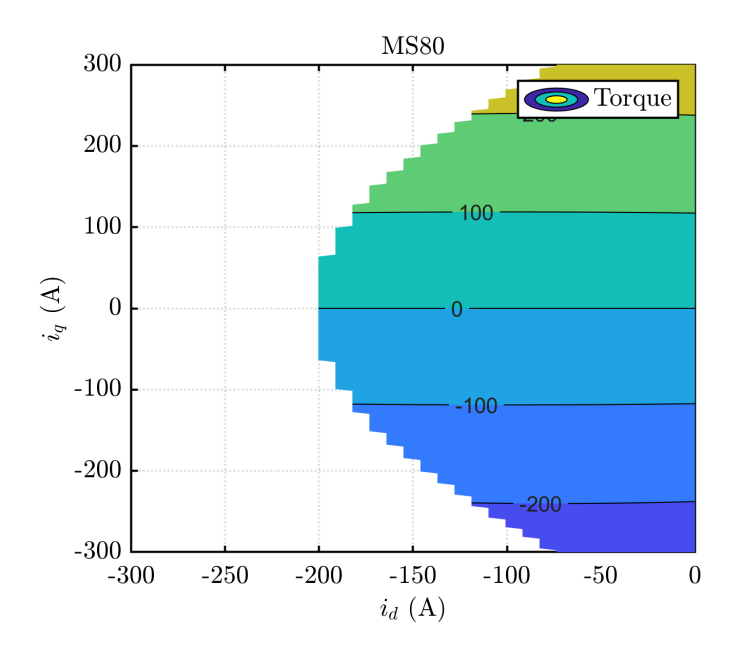


Figure 3.10: Iso-torque for MS80

These analyses laid the groundwork for assessing the machine's operational limits, including the voltage constraints during the remagnetization process, which are critical for defining feasible control strategies and ensuring reliable performance in real-world applications.

3.3 Remagnetization voltage limit

Every electric machine is subject to a voltage limit imposed by the maximum voltage the inverter can supply. In Variable Flux Machines (VFMs), this constraint becomes particularly critical during remagnetization operations, as the required currents are significantly high. It is therefore essential to verify that these operations can be performed without exceeding the maximum available voltage.

Near this limit, the machine voltage can be approximated as the product of the magnetic flux and the electrical angular frequency.

$$|\mathbf{v}_{dq}| \approx \omega \cdot \lambda$$
 (2)

Consequently, the constraint condition can be expressed by imposing that this voltage does not exceed the maximum voltage deliverable by the inverter, which is equal to $V_{max} = v_{DC-link}/\sqrt{3}$.

$$|\boldsymbol{v}_{dq}| \le V_{max} \tag{3}$$

The maximum available flux is therefore obtained by dividing this voltage by the electrical angular frequency,

$$\lambda_{max} = \frac{V_{max}}{U} \tag{4}$$

which in turn depends directly on the rotor mechanical speed, the number of pole pairs, and the $\pi/30$ factor.

$$\omega = n \cdot p \cdot \frac{\pi}{30} \tag{5}$$

Using SyR-e, it was possible to extract a curve, referred to as the Remag Curve, that represents the flux required to remagnetize the machine to a specific Magnetization State (MS) level while maintaining constant torque (Fig.3.11).

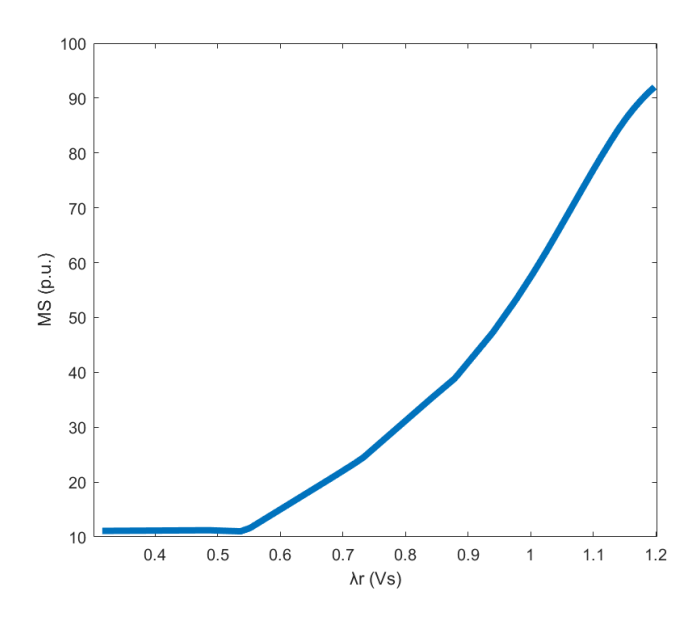


Figure 3.11: MS vs λ Remag curve

This curve allows the determination, for any given rotational speed, of the maximum MS achievable without violating the voltage constraint. The procedure involves first calculating the maximum available flux at that speed, then identifying the corresponding MS level on the remagnetization curve and finally interpolating the previously obtained T–n curves to estimate the associated torque.

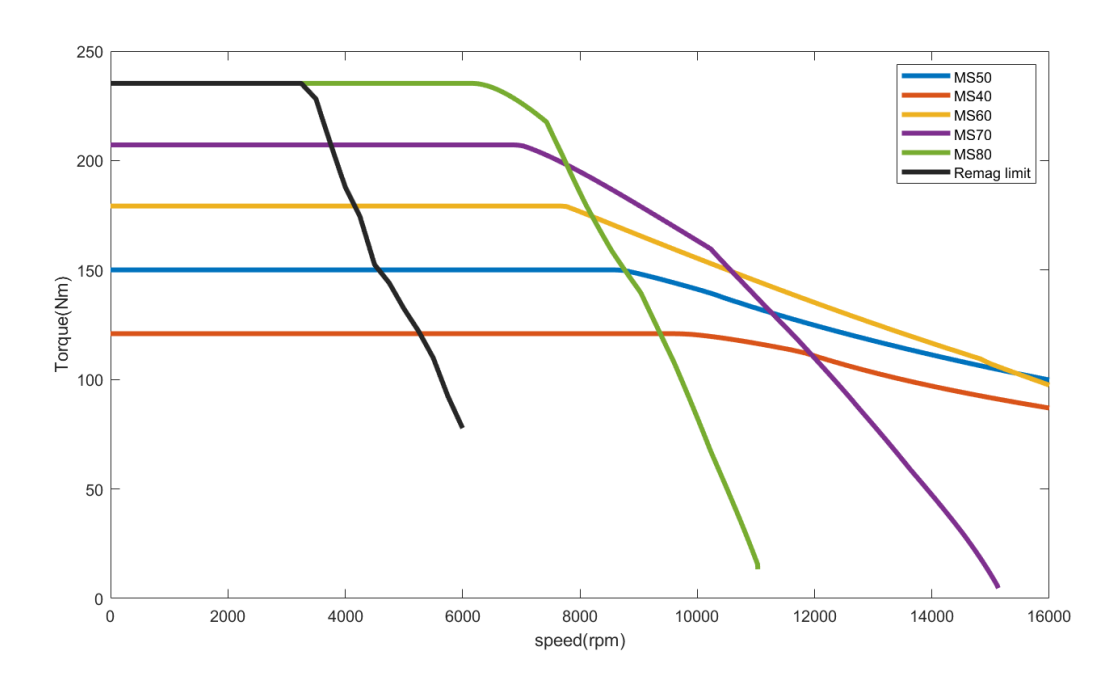


Figure 3.12: T-n curves with Remag voltage limit

The outcome of this analysis is shown in Fig.3.13, which presents the Remagnetization Limit Curve (the black line). This curve defines the safe operating region for remagnetization, highlighting that it is only possible to transition from a lower MS to a higher MS if the operating point lies below this curve, i.e., at speeds lower than the imposed limit. Conversely, this constraint is not present during demagnetization, as the currents involved are significantly smaller.

A practical example clarifies this behavior: if the motor initially operates at MS = 80%, it can be accelerated along its corresponding curve until it intersects the curve of MS = 40%, continuing to demagnetize the magnet as the speed increases. However, during deceleration, it is not possible to return directly to the MS = 80% curve, as this would violate the voltage limit. Instead, the motor must continue to operate along the MS = 40% curve until the speed drops below the threshold defined by the Remag Limit; only then can remagnetization occur, raising the MS back to a higher level.

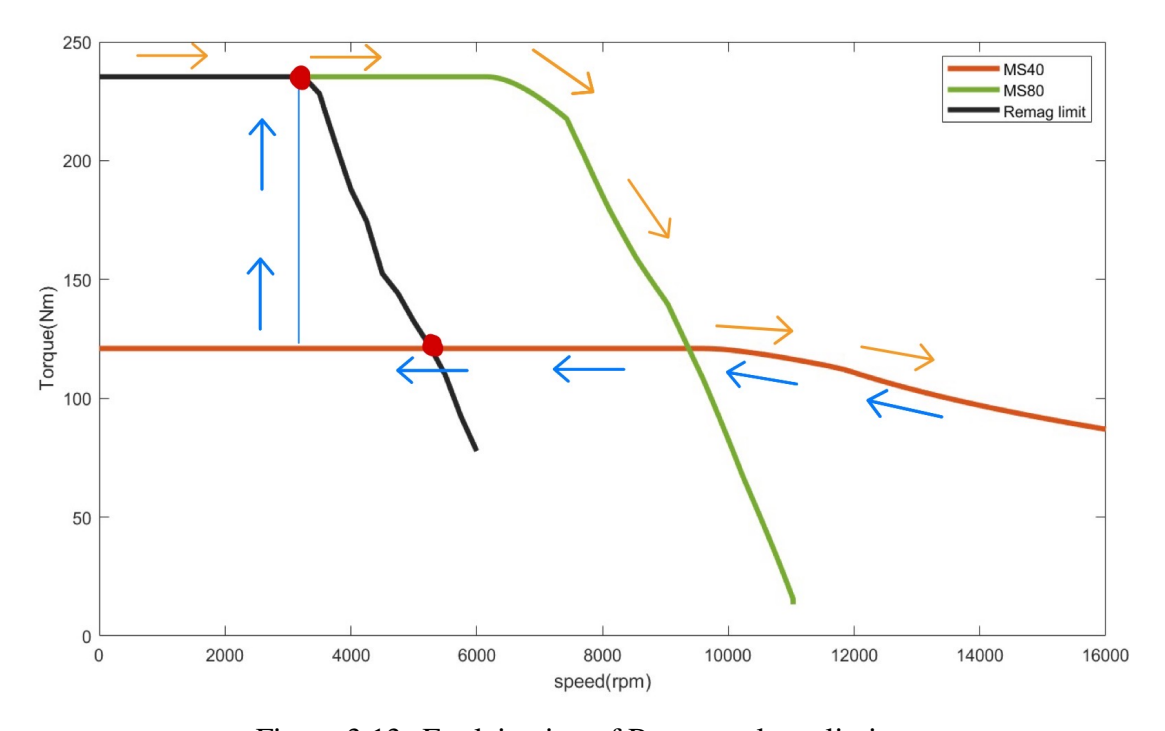


Figure 3.13: Explaination of Remag voltage limit

This constraint introduces significant complexity in motor management, particularly in typical automotive drive cycles, where frequent torque and speed variations make it challenging to ensure smooth transitions between different magnetization states. One potential mitigation strategy is to adopt a multi-step approach, performing the transition from a low MS to a high MS through intermediate stages. Although this method can partially alleviate the issue, it requires

a greater number of current pulses, thereby increasing control complexity and overall energy losses [9].

3.4 Efficiency maps

Efficiency maps were computed using JMAG for different magnetization states, ranging from MS = 40% to MS = 80%. The procedure began with a preliminary demagnetization study, which was required to set the machine at the desired MS level for the subsequent analysis. Once the magnetization state was established, the efficiency map was generated through an Accuracy Priority study (Fig. 3.14), making use of the Reuse Demagnetization condition (discussed in the previous chapter). This option allowed the magnetization state obtained in the initial study to be directly reused, thereby significantly reducing simulation time while preserving accuracy.

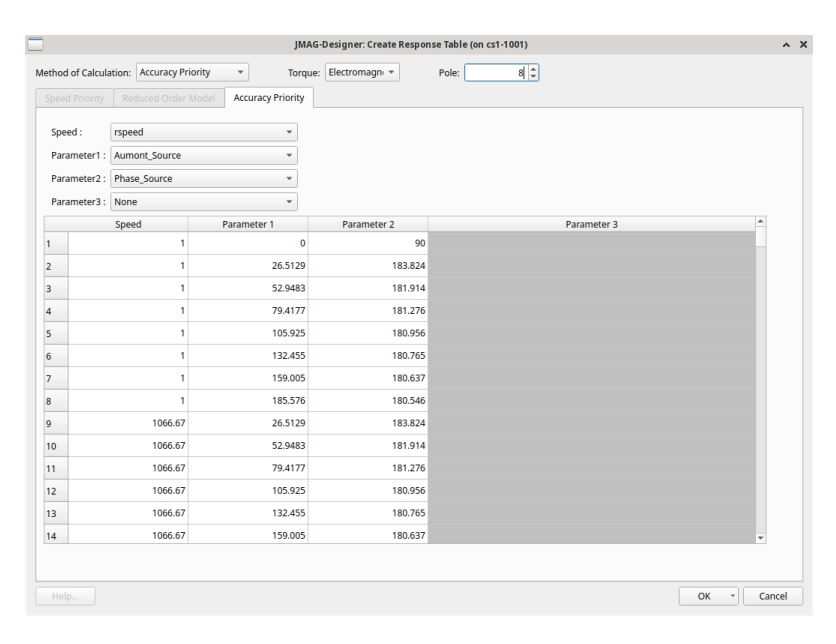


Figure 3.14: Accuracy priority setup

The maps were created by calculating efficiency at a discrete set of operating points within the torque—speed curve of the respective MS. A differentiated sampling strategy was adopted: a denser grid in the low-torque region (0–80 Nm), as this is the most frequently used operating area in automotive applications, and a coarser grid in the range between 80 Nm and the maximum torque achievable at that MS level (Fig. 3.15). The results were then interpolated to obtain the complete efficiency map. Finally, the computed data were imported into MATLAB for post-processing and for the generation of the corresponding loss maps, thus providing a comprehensive overview of the machine's energy behavior across different magnetization states.

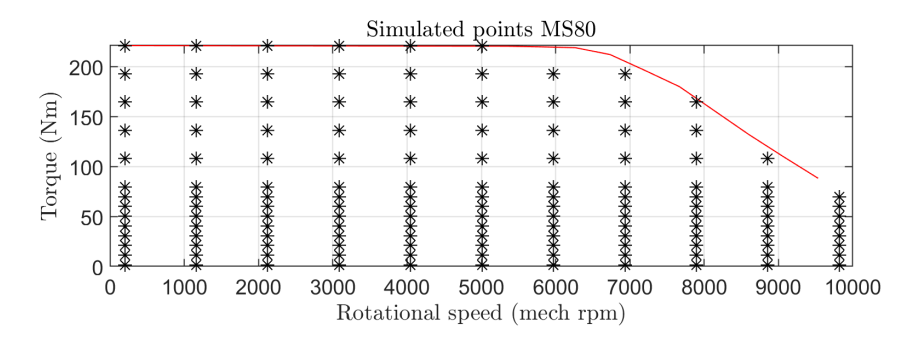


Figure 3.15: Simulated points for MS80

A particularly important result, shown in Fig. 3.16, is that as MS decreases, the region of maximum efficiency shifts towards higher speeds at constant torque. This effect highlights the benefit of flux modulation in extending the operational flexibility of the machine and optimizing performance across different driving conditions.

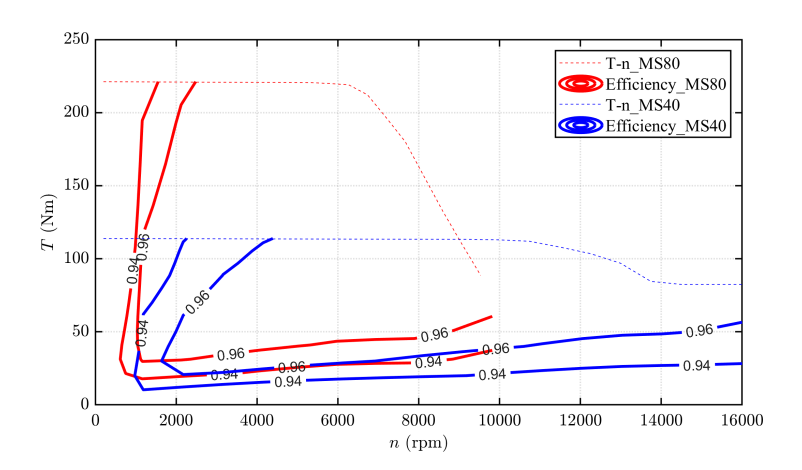


Figure 3.16: Efficiency variation

The resulting maps are presented in the following figures.

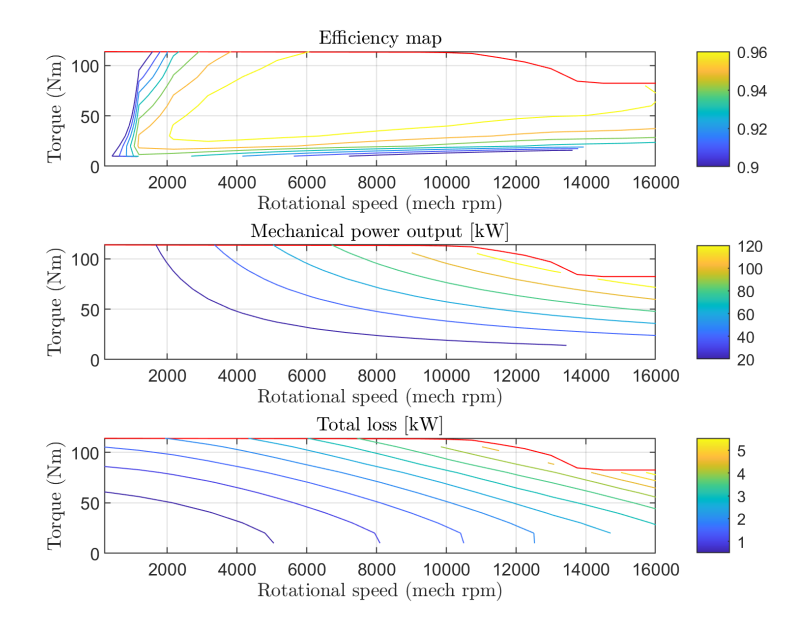


Figure 3.17: Efficiency map for MS40

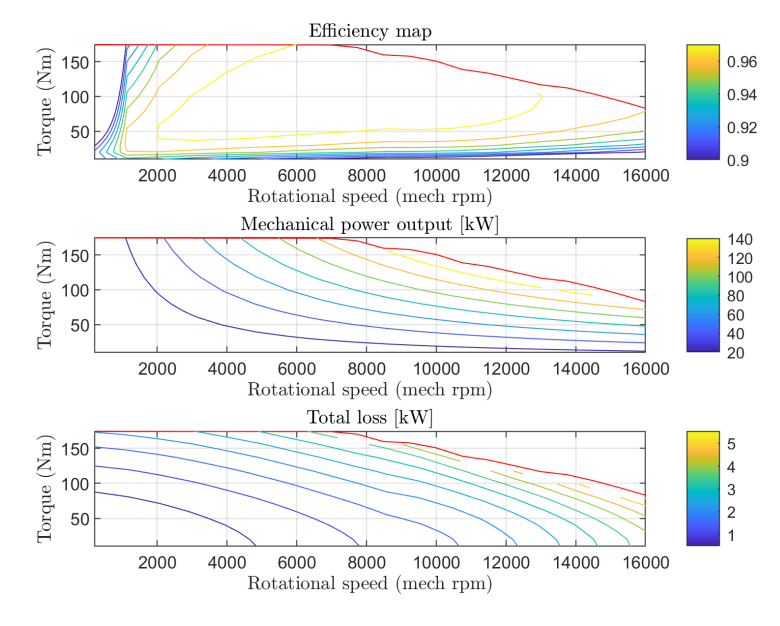


Figure 3.18: Efficiency map for MS60

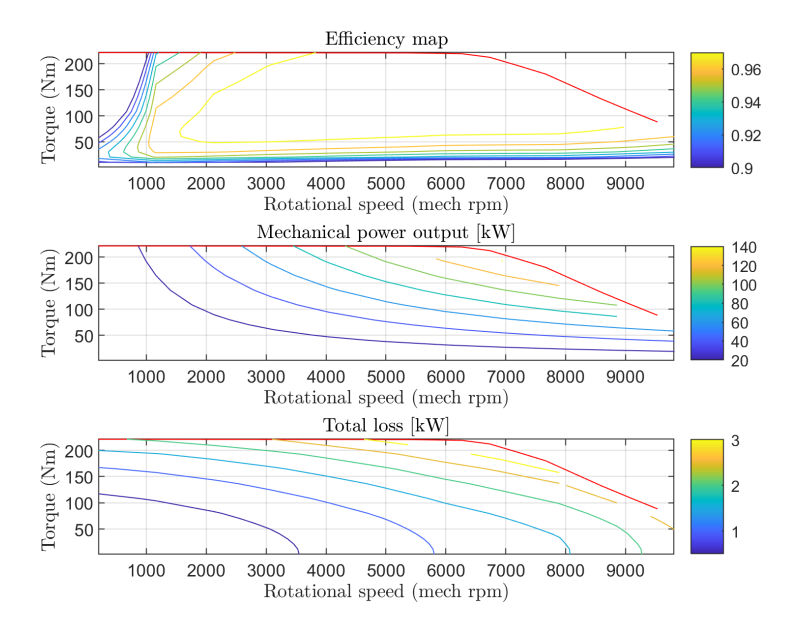


Figure 3.19: Efficiency map for MS80

In conclusion, the efficiency map analysis demonstrated that the controlled variation of the magnetization state (MS) has a strong impact on the machine's energy performance. Specifically, decreasing MS results in a shift of the high-efficiency region towards higher speeds, enabling better adaptation of the machine to the operating conditions of typical automotive drive cycles. These findings confirm the potential of variable flux machines to enhance operational flexibility and overall system efficiency, while also providing valuable insights for the development of advanced control strategies.

3.5 Drive Cycle

To assess the machine's dynamic performance under realistic operating conditions, a drive cycle simulation was carried out using a reference vehicle. The chosen driving profile was the WLTC (Worldwide harmonized Light vehicles Test Cycle), shown in Fig.3.24.

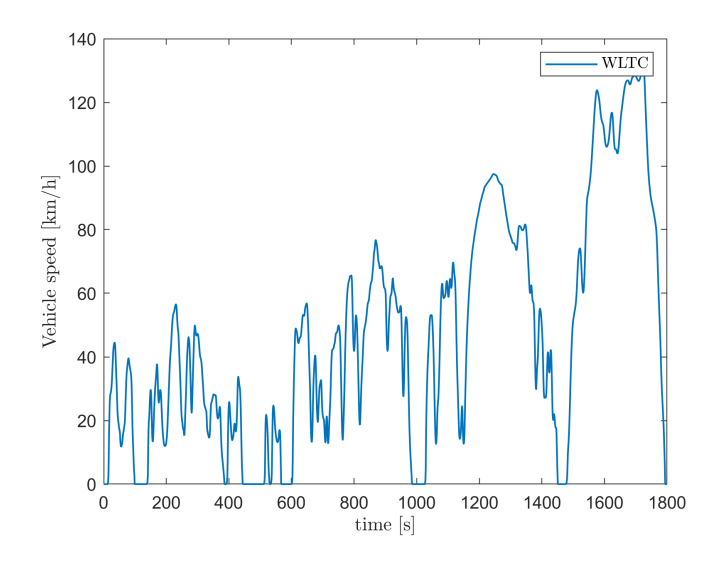


Figure 3.20: WLTC Drive Cycle

In the first scenario, the simulation was performed with only two available magnetization states: MS = 80% and MS = 40%. The results demonstrate that the vehicle was able to complete the entire cycle without violating any design constraints: there were no instances where the maximum torque limit (black line) was exceeded, nor situations where the remagnetization limit (purple line) was surpassed. The machine operated mostly at MS = 80%, with a switch to MS = 40% required only in the final high-speed deceleration phase. As highlighted in the torque–speed map, the last operating points (blue) were not enclosed within the torque envelope of MS = 80%, but were fully contained within that of MS = 40%. At the end of the cycle, the transition back to MS = 80% occurred without issues, since it took place below the speed threshold imposed by the Remag Limit (3200 rpm).

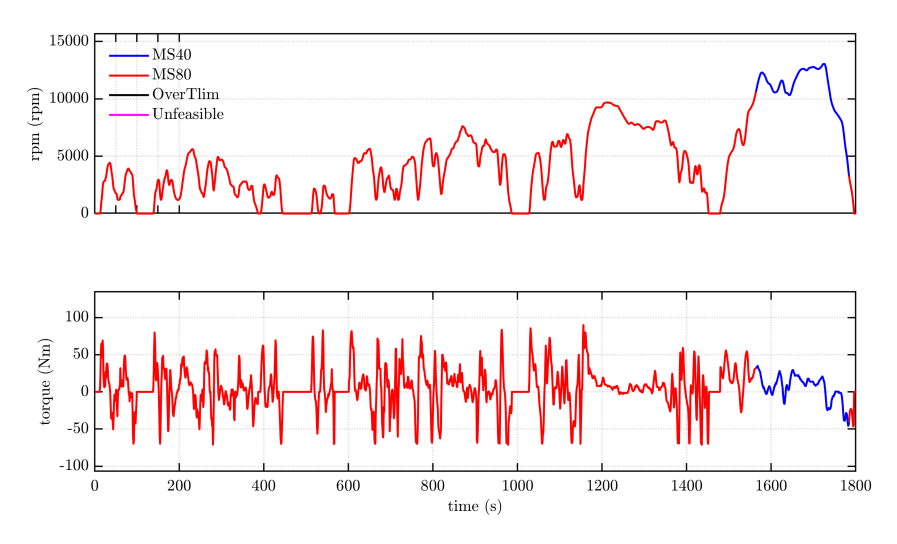


Figure 3.21: WLTC Drive Cycle, two MS scenario (MS40, MS80)

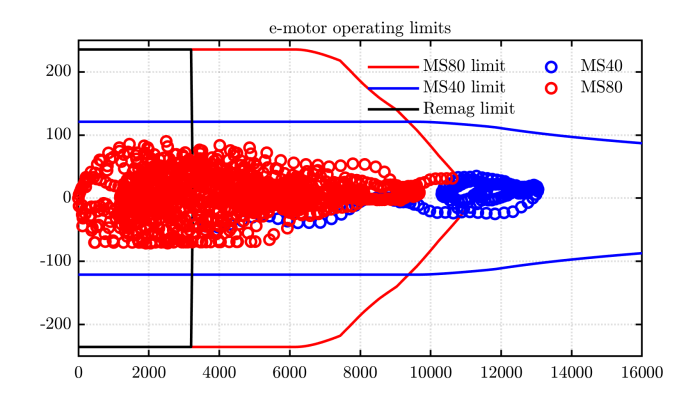


Figure 3.22: WLTC working points, two MS scenario (MS40, MS80)

A second case was then investigated, introducing three magnetization states: MS = 80%, 60%, 40%. In this configuration, the remagnetization limits were found to be approximately 3200 rpm for MS = 80% and 4200 rpm for MS = 60%. Once again, the vehicle successfully completed the WLTC cycle without constraint violations. Interestingly, the MS = 40% state was never engaged, as all operating points remained within the torque curve corresponding to MS = 60%, making the alternation between MS = 80% and MS = 60% sufficient to cover the entire drive cycle.

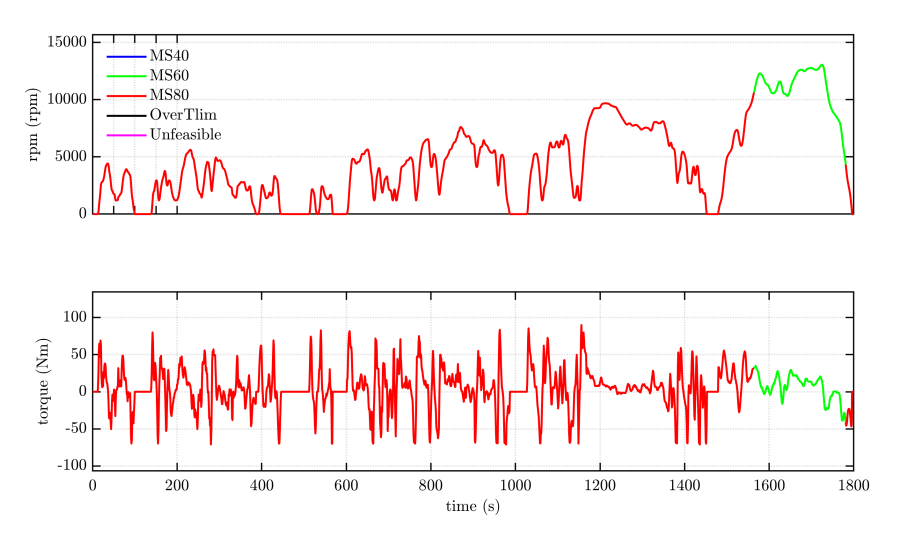


Figure 3.23: WLTC Drive Cycle, three MS scenario (MS40, MS60, MS80)

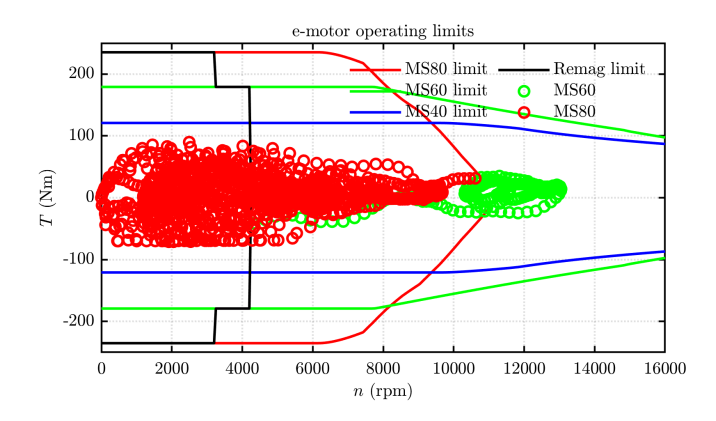


Figure 3.24: WLTC working points, three MS scenario (MS40, MS60, MS80)

3.6 Cost Analysis and Environmental Load Unit (ELU)

To complete the study, a cost analysis and an environmental impact evaluation through the Environmental Load Unit (ELU) were carried out. As shown in the table, the designed machine exhibits considerable size and weight, with a total mass close to 50 kg. This is mainly the result of design choices made during the optimization process, where both the rotor diameter and the axial length of the machine were increased in order to meet the required performance specifications.

Part	Weight [kg]
Windings	5.52
REE Free Magnet	2.39
Rotor	14.34
Stator	25.28
TOTAL	47.53

Figure 3.25: Volume and weight contribution of each motor part

While these modifications enabled the achievement of the target performance, they also led to higher overall costs compared to the benchmark machine. The analysis therefore highlights that the optimized configuration is economically more demanding.



Figure 3.26: Cost Analysis

On the environmental side, expressed in terms of ELU, the difference between the benchmark and the optimized design is less pronounced. This outcome is due to the fact that, although the developed machine requires a higher amount of copper, it does not contain neodymium. Since neodymium is associated with a very high ELU per unit mass, its elimination significantly reduces the environmental impact, partially compensating for the increase caused by the larger copper content.

Material	Deviation from Benchmark (ELU)
Cu	298.7
Laminate	47.2
Iron Nitride	0.7
N42UH	-71.4
Total Magnets	-70.7
Total ELU	275.2

Figure 3.27: Deviation from Benchmark

3.7 Conclusion and Future Works

In this thesis, a design methodology for a Variable Flux Machine (VFM) intended for automotive applications was developed and validated, with the primary goal of reducing the use of rare earth elements while maintaining competitive performance in terms of torque, efficiency, and controllability. The work was carried out in collaboration with Volvo Cars, which provided the initial reference model and helped frame the project within an industrially relevant context for sustainable mobility.

The methodology combined two complementary tools: JMAG, employed for advanced modeling and optimization through finite element analysis, and SyR-e, used for the automated generation of flux, torque, and efficiency maps as well as for the evaluation of the machine's magnetic behavior. Through a sequence of iterative phases, a coherent workflow was established, starting from parametric modeling, proceeding with multi-objective optimization, and culminating in the detailed analysis of constraints and control strategies.

The results confirmed the effectiveness of the proposed design methodology, demonstrating that the VFM can adapt to different operating conditions while maintaining strong overall performance. Simulations showed that it is possible to modulate the magnetization state to extend the speed range and improve system efficiency at operating points typical of automotive drive cycles.

A key outcome of the study was the identification of the voltage limit as a critical constraint for remagnetization, highlighting the need for more sophisticated control strategies, such as gradual transitions between magnetization states. Furthermore, WLTC drive cycle simulations demonstrated that the optimized VFM design can satisfy real driving conditions without violating torque or voltage constraints. The use of multiple magnetization states allowed the machine to flexibly adapt to varying torque and speed demands, ensuring both efficiency and robustness.

The cost and environmental impact analysis revealed an important trade-off: while the optimized design requires a larger amount of copper and results in higher costs compared to the benchmark, it eliminates neodymium entirely. This represents a significant sustainability advantage, as confirmed by the Environmental Load Units (ELU) analysis, where the absence of rare earths offsets the increased copper usage.

In conclusion, this work demonstrated the feasibility of a rare-earth-free VFM design methodology, highlighting both its environmental benefits and the challenges related to control and dynamic performance. The strategies developed represent a step toward the advancement of more sustainable electric machines tailored to future mobility. Future research could focus on further geometry optimization to reduce weight and cost, the development of more robust control algorithms to manage the Remagnetization Voltage Limit, and the extension of validation to experimental testing on physical prototypes, thereby consolidating the simulation results and moving the technology closer to industrial implementation.

References

- [1] W. Zhang and W. Xu, "An improved variable flux memory machine topology with multi-stage magnetization strategy," *IEEE Transactions on Applied Superconductivity*, vol. 34, no. 8, pp. 1–5, 2024.
- [2] R. Fathi and G. A. Markade, "A review of variable flux motors: Design, control, and applications," in 2025 16th Power Electronics, Drive Systems, and Technologies Conference (PEDSTC), 2025, pp. 1–8.
- [3] M. S. Mirazimi, C. Chen, P. Pescetto, S. Ferrari, G. Pellegrino, M. Diana, and T. Thiringer, "Accurate modeling of variable- flux pmsms without electromagnetic co-simulation," in 2024 International Symposium on Power Electronics, Electrical Drives, Automation and Motion (SPEEDAM), 2024, pp. 625–630.
- [4] H. Hua, H. Ge, and W. Hua, "Multi-objective hierarchical optimization of variable flux memory machines with diverse operation conditions," in 2024 International Conference on Electrical Machines (ICEM), 2024, pp. 1–6.
- [5] Q. Wei, Z. Zhu, Y. Jia, J. Feng, S. Guo, Y. Li, and S. Feng, "Electromagnetic performance analysis of variable flux memory machines with series-magnetic-circuit and different rotor topologies," *CES Transactions on Electrical Machines and Systems*, vol. 8, no. 1, pp. 3–11, 2024.
- [6] C. Chen, *Variable flux permanent magnet machines for sustainable traction electrification*, PowerPoint presentation, 2025.
- [7] S. Ferrari, F. Cupertino, and G. Pellegrino, *SyR-e Software*, 2014. [Online]. Available: https://github.com/SyR-e.
- [8] S. Ghiba, "Design of a cost effective ipm machine minimizing the use of rare earth magnets," Master Thesis, Politecnico di Torino, Torino, Italy, 2024.
- [9] C. Chen, P. Pescetto, S. Ferrari, G. Falk Olson, M. Diana, T. Thiringer, and G. Pellegrino, "Fast determination of feasible torque-speed range for variable flux machines including remagnetization voltage limit," 2025.